frontiers | Frontiers in Environmental Engineering

TYPE Review
PUBLISHED 01 November 2023
DOI 10.3389/fenve.2023.1228992

OPEN ACCESS

EDITED BY
Zacharias Frontistis,
University of Western Macedonia, Greece

REVIEWED BY
Maria Laura Tummino,
National Research Council of Italy (CNR), Italy
Bampos Georgios,
University of Patras, Greece

*CORRESPONDENCE
Liangdong Fan,
fanld@szu.edu.cn
Kristina Mikhailovna Maliutina,
maliutinak@cardiff.ac.uk
Andrea Folli,
follia@cardiff.ac.uk

RECEIVED 25 May 2023
ACCEPTED 04 September 2023
PUBLISHED 01 November 2023

CITATION
Maliutina KM, Omoriyekomwan JE, He C, Fan L and Folli A (2023), Biomass-derived carbon nanostructures and their applications as electrocatalysts for hydrogen evolution and oxygen reduction/evolution.
Front. Environ. Eng. 2:1228992.
doi: 10.3389/fenve.2023.1228992

Biomass-derived carbon nanostructures and their applications as electrocatalysts for hydrogen evolution and oxygen reduction/evolution

Kristina Mikhailovna Maliutina [1,2,3]*, Joy Esohe Omoriyekomwan [4], Chuanxin He [1,2], Liangdong Fan [1,2]* and Andrea Folli [5]*

[1]Department of New Energy Science & Technology, College of Chemistry and Environmental Engineering, Shenzhen University, Shenzhen, Guangdong, China, [2]College of Physics and Optoelectronic Engineering, Key Lab of Optoelectronic Devices and Systems of Ministry of Education/Guangdong Province, Shenzhen University, Shenzhen, Guangdong, China, [3]School of Chemistry, Cardiff University, Cardiff, United Kingdom, [4]Key Laboratory of Advanced Coal and Coking Technology of Liaoning Province, School of Chemical Engineering, University of Science and Technology Liaoning, Anshan, China , [5]School of Chemistry, Net Zero Innovation Institute, Cardiff Catalysis Institute, Cardiff University, Cardiff, United Kingdom

Biomass derived electrocatalysts with rationally designed activity, selectivity, and stability present a major sustainable approach for the electrochemical production of fuels and value-added chemicals. This review presents recent advances in the field of biomass-derived electrocatalytic nanostructures for the hydrogen evolution reaction (HER) and the oxygen reduction and evolution reactions (oxygen reduction reaction and oxygen evolution reaction), that are subject of major research efforts, as well as public and private investment, as they will play a crucial role in the energy transition and in achieving net zero carbon emissions. The review summarises experimental and theoretical investigations aiming at tuning electrocatalytic performances of sustainable C-based nanostructured materials, and present opportunities for future commercialization of innovative energy materials and applications. In reviewing relevant literature in the field, we focus on the correlation between electrocatalytic activity/selectivity and synthesis methods, composition, physical chemical characteristics, in the attempt to uncover a clear structure-activity relationship. Furthermore, this study provides a critical comparison of the different electrocatalysts in light of their catalytic mechanisms, limiting phenomena, and practical applications for sustainable future technologies.

KEYWORDS

carbon nanomaterials, electrochemistry, biomass-derived electrocatalyst, heteroatom doping, active sites engineering

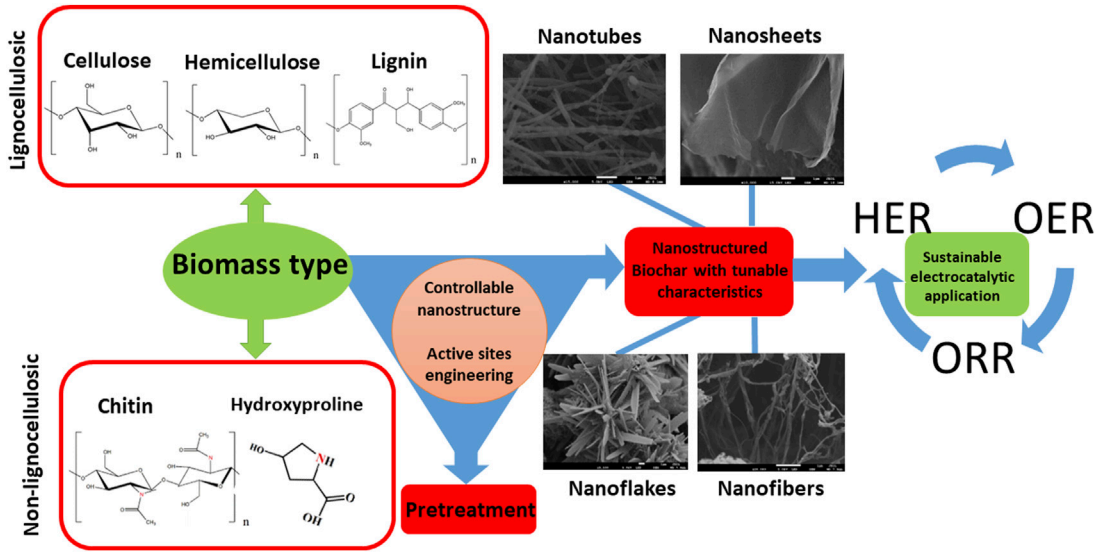

GRAPHICAL ABSTRACT

Highlights

- Carbon nanomaterials from biomass for electrocatalytic application were summarized
- Determination of structure-to-activity relationship from biomass and their precursors
- Pretreatment is a crucial step towards nano-microstructural engineering
- Actual active sites through non-metal and metal doping based on electrochemical figures of merit
- Integration of computational and experimental studies is highly desired

1 Introduction

Continuous disruptive impact on nature, climate change, environmental crisis, and energy shortage has shifted the research community attention towards pursuing non-hazardous, sustainable and renewable energy conversion and storage. Since the second half of the 20th Century, electrochemical transformations of small, molecules such as H_2O, O_2, N_2, as well as greenhouse gases such as CO_2, CH_4, and N_2O, into fuels and value-added chemicals have increasingly dominated the field of electrochemistry. Electrochemical water splitting and electrochemical hydrogen evolution reaction (HER) for hydrogen production had already been demonstrated in the 19th Century by Nicholson and Carliste (Kreuter and Hofmann, 1998). A second major milestone was achieved in the 1960s with the report on the electrochemical CO_2 reduction reaction (CO_2RR) by Jordan and Smith (Jordan and Smith, 1960; Meshitsuka et al., 1974), followed 30 years later, by the work of Hori and co-workers on the possibility of producing chemicals and fuels using this process (Hori et al., 1985; Hori et al., 1986; Hori et al., 1989). As of today, more than 30,000 research articles have been published on electrochemical transformations such as HER and CO2RR. Despite major recent developments, and deployment of industrial scale electrolysers for water splitting and H_2 production, these electrochemical processes are confronted with the shortcoming of electrocatalysts based on rare and expensive noble metals as the bottleneck toward practical implementation.

A promising alternative for conventional fossil fuels and combustion engines is next-generation energy production/conversion/storage technologies, such as fuel cells (FCs), electrolytic cells, water splitting systems, capacitors and batteries that generate clean, eco-friendly electricity by electrochemically reducing O_2 and oxidizing a fuel, i.e., H_2, into water. FCs are small in size, silent energy conversion devices that directly convert the chemical energy of different fuels into electrical energy at a much promising efficiency, both theoretically and practically, as compared to conventional power generation sources (Fan et al., 2018; Sayed et al., 2019; Abdelkareem et al., 2021). Recent FC technologies includes alkaline membrane fuel cells (AMFCs), solid (or solid-state) alkaline fuel cells (SAFCs), hydroxide exchange membrane fuel cells (HEMFCs), alkaline polymer electrolyte fuel cells (APEFCs) and polymer electrolyte alkaline fuel cells (PEAFCs) (Dekel, 2018). For instance, a proton exchange membrane fuel cell (PEMFC) fuelled by hydrogen generates water as a byproduct, with a small release of waste heat. This is very promising compared to the huge gaseous emissions, waste heat, and cooling demand in conventional power generation systems. Microbial FCs are another class of devices that utilize microbes, hence, more environmental-friendly and eco-sound with a wide range of applications, ranging from power generation to desalination.

Once again, bottlenecks hindering global applicability and scale up are large amounts of noble metal electrocatalysts, durability, as well as overpotentials required for the HER (Tang et al., 2018a; Tang et al., 2018b; Tang et al., 2019), oxygen reduction reaction (ORR)

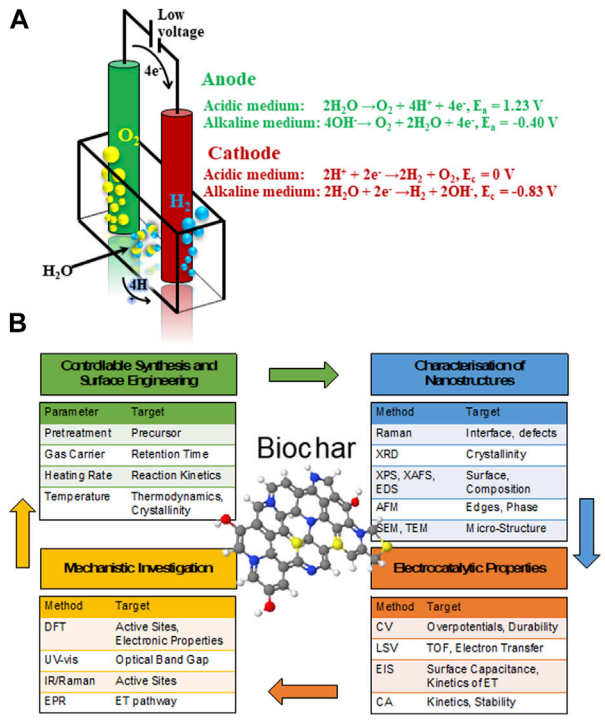

FIGURE 1
Schematic diagram of **(A)** representation of a water splitting electrolytic cell and **(B)** multistep approach for rational synthesis and characterization of biomass-derived carbon nanocarbons for electrochemical application.

(Shao et al., 2016; Fan et al., 2018; Li F. et al., 2020; Maliutina et al., 2021a; Li et al., 2023) and oxygen evolution reaction (OER) (Li et al., 2021; Huang et al., 2022).

J. R. Deiman and Adriaan Paets van Troostwijk demonstrated a water electrolysis in 1789, while a typical electrolytic cell for water splitting is illustrated in Figure 1A (Wang J. et al., 2020). The water splitting process involves two half-cell reactions: anodic oxidation or oxygen evolution reaction (OER) and cathodic reduction or HER, respectively. The recent insights on electrochemical mechanisms in both alkaline and acidic environments are highlighted in details in the Supporting Material (SI). However, efficient catalysts are desired to overcome the sluggish kinetics and large overpotential of these electrochemical reactions. Nevertheless, the scarcity, high cost and poor tolerance of widely employed standart platinum group metals-based electrodes severely hinder a large-scale applications of fuel cells and water splitting devices.

The development of abundant, stable and low-cost electrocatalysts as cathode material is a colossal issue (Nie et al., 2015). Recently, many researchers shifted attention towards Earth abundant alternatives to noble metals, such as carbon-based electrocatalysts (Zhang Y. et al., 2016; Borghei et al., 2017; Zhang et al., 2018). Among various carbonaceous assemblies, carbon nanomaterials (CNs) are recognized amongst as potentially active and versatile electrocatalysts with a good degree of tunability of their physical chemical properties. Heteroatom-doped graphene (Wang S. et al., 2012), thin carbon nanosheets (Jiang et al., 2019a), carbon nanotubes (CNTs) (Gong et al., 2009; Maliutina et al., 2021a) and nanofibers (CNFs) (Wu M. et al., 2018) and recently synthesized graphdyine (Zhao et al., 2018) are amongst the emerging C-based materials being investigated as promising electrocatalysts.

The potential of using biomass to produce such C-based materials for electrocatalysis has recently been investigated (Chen et al., 2014; Ye et al., 2015; Zhang Y. et al., 2016; Huang et al., 2017; Cheng et al., 2021), including challenges associated to their complex and non-regular organic structure (Khiari et al., 2019; Munawar et al., 2021). Several studies have illustrated different pretreatment pathways of biomass, including alkaline, acidic, hypersaline and a variety of extraction methods for fabrication of advanced nanomaterials, such as pyrolysis and carbonization with controllable and reproducible carbon structure (Prakash Menon et al., 2017; Omoriyekomwan et al., 2019; Maliutina et al., 2021b). However, a clear understanding on how to rationally design nanostructured electrocatalysts with desired structure and activity from biomass is lacking, in great part due to the difficulty of standardising synthetic procedures. This is mostly due to the substantial variability of different biomass sources in terms of chemical composition and structure. Systematically reviewing the major achievements in biomass-derived nanomaterials for electrocatalytic applications, in particular HER, ORR, and OER, can help to unravel interesting trends and correlations that would improve the way we engineer improved kinetics and mechanisms of electrocatalytic processes based on biomass derived nanostructured electrocatalysts (Figure 1B). This review presents a comprehensive comparison and discussion on how starting biomass feedstocks influence final electrocatalyst active sites, electronic properties and performances, and evaluates crucial aspects such as biomass pretreatment methods as well as synthetic conditions.

Particular attention is given to the role of biomass sources, composition, and physical chemical properties determining morphologies and electronic structure of the final electrocatalysts. We also examine the impact of heteroatom doping on electrocatalytic activity and mechanisms that over the last few years have emerged as a strategy to further improve electrocatalytic performances (Borghei et al., 2017; Li Y. et al., 2019; Zhou et al., 2020). Finally, we propose outlook and perspectives on future applications of biomass-derived C-based electrocatalysts.

2 The role of biomass variability on the yield and structure of C-based materials

2.1 Biomass as a source for advanced carbon-based nanomaterials

According to the classification proposed by Vassilev et al., biomass is a non-fossil, complex and biogenic heterogeneous mixture of organic and inorganic matter that is primarily generated by photosynthesis, such as natural constituents from lands and water-based vegetation; animal or human food digestion; anthropogenic processing of wood, plants and other organic matter, such as manure or household waste (Vassilev et al., 2010). Biomass is typically utilized for solid, liquid and gaseous products from non-edible residues formed by floras and faunas, such as corn cobs, wheat stalk, cornstalk, and manure (Supplementary Table S1). Biomass is carbon-rich, sustainable,

and renewable. This has made it a sought-after precursor for generating green CNs (solid component) as well as being used for the production of value-added chemicals and biofuels (predominantly liquid and gaseous component) (Bhaskar et al., 2011; Titirici et al., 2015; Anca-Couce, 2016; Kumar et al., 2016).

Biomass can be divided into two major groups with the same characteristics of origin and chemical structure, i.e., lignocellulosic and non-lignocellulosic biomass (Martin, 2010; Kosinkova et al., 2015).

Lignocellulosic biomass is considered one of the most promising renewable sources for producing carbon materials and fuels while remaining environmentally friendly (Cai et al., 2015; Kabir and Hameed, 2017; Li et al., 2017). Lignocellulosic biomass is mainly a waste of wooden and crop industries; primarily rich in hemicellulose (15%–40%), cellulose (25–50 wt%), and lignin (10%–40%) (Chen, 2014; Kumar et al., 2016; Maliutina et al., 2017; Li Y. et al., 2020).

Cellulose is a linear polysaccharide that unsoluble in water and consists of D-glucose monomers bonded together via β-(1–4) glycosidic bonds (Abraham et al., 2011). The inter and intramolecular hydrogen bonds that give cellulose its crystalline form are formed between the three hydroxyl groups on each glucose monomer (Harmsen et al., 2010). Cellulose microfibrils are formed due to the coalescence of the polymer chains to form fibers, which in turn gives cellulose its crystalline structure (Shafizadeh, 1982). Hemicellulose comprises of various monomers such as glucose, mannose, arabinose, and xylose, which vary in quantity according to the type of biomass (Li, 2014). Hemicellulose take place in association with cellulose in the cell wall, but unlike cellulose, hemicelluloses are soluble in dilute alkali. Hence, xylan, which is the most abundant monomeric hemicellulose unit up to about 10% and 30% of the dry weight of the species (Yaman, 2004). Unlike cellulose, hemicellulose does not exhibit a crystalline structure due to the high number of branched chains and acetyl groups linked to a polymer chain. Lignin is an aromatic polymer in nature that consists of p-coumaryl, coniferyl, and sinapyl alcohol monomers and hydroxyl, carbonyl, and methoxy functionalities to form a firm composition (Chen, 2014). During pyrolysis or carbonization processes, hemicellulose decomposition occurs first at 200°C–260°C. Cellulose fragments and lignin structure break up at 240°C–350°C (Wang et al., 2015) and 280°C–500°C (Ramanayaka et al., 2020), respectively. The ratio of every single compound of hemicellulose, cellulose, or lignin is not regular and constant, which is related to the species, age, soil, place of origin (Liu et al., 2019).

Non-lignocellulosic biomass is predominantly comprised of carbohydrates, lipids, proteins and inorganic minerals (Li and Jiang, 2017). Apart from algal biomass, non-lignocellulosic type includes animal hair, feathers, bones, fish and seafood waste, sewage sludge, and manure (Li and Jiang, 2017). Sewage sludge encompasses different constituents like organics, inorganics, and microbes (Yu et al., 2021). Algae is considered a significant component of the Earth's biomass, whose growth rate and CO_2 fixation effectiveness are higher than any earthly plant (Zhao et al., 2015). Algae consist mainly of lipids, proteins, ash, and carbohydrates. The main elements in algae are C and O, which account for 25%–55% and 15%–50%, while H and N are accounts for 5%–10% of algae, respectively (Li et al., 2017).

The conversion of biomass to advanced nanostructures is influenced by source, physical and chemical composition, that is highly variable in terms of origin and growth factors (e.g., environment) which can either enrich or deplete different compounds and elements (Vassilev et al., 2015). On average, the elemental composition of biomass consists of 99.9% of C, Ca, Cl, H, K, Mg, N, Na, O, P, and S, with ≤0.1% of trace elements (Vassilev et al., 2013). In summary, biomass has proven to be the an ideal source for CNs, given a series of advantages, including its relatively low cost and worldwide abundance; the absence of competition with the food industry; the natural viability of N, S, P, and O, allowing for doping and formation of chemical functionalities, without the need of extra chemicals.

2.2 Biochar

Biochar is a carbon-rich material that is produced by heating organic matter, such as wood chips, agricultural waste, or manure, in an oxygen-depleted atmosphere (Li Z. et al., 2019). The chemical nature of biochar is complex and depends on the type of biomass used, the thermal treatment conditions, and the post-treatment processes. Biochar is predominantly composed of carbon, with content ranging from 50% to 95% depending on the production process (Li Y. et al., 2020). The carbon in biochar is present in various forms, including elemental carbon, amorphous carbon, and graphite-like structures. These different forms of carbon are distributed throughout the biochar, creating a porous structure that provides high surface area and high adsorption capacity (Omoriyekomwan et al., 2021a). Apart from C, biochar also contains other elements such as H, O, N, and S, which are present in smaller quantities, and that can be included in C-based structures as dopants (Maliutina et al., 2018). The elemental composition of biochar significantly depends on the type of biomass used and the production conditions (Maliutina et al., 2017).

Biochar also contains a range of functional groups, such as carboxylic acids, phenols, ketones, and aldehydes. These functional groups are in large extent responsible for biochar chemical reactivity. The possibility of rationally designing these types of moieties on biochar surfaces presents a powerful strategy for tuning their potential catalytic properties, as well as influencing the adsorption of ions and molecules in the environment, by adjusting the overall acidity and basicity of the biochar surfaces. The surface area and porosity of biochar are further crucial features influencing chemical and catalytic properties. The porous structure of biochar is ordinarily emerging from the thermal preparation process, when the volatile constituents in the biomass are released, leaving behind a charred residue (Sch et al., 2011). Once again, the possibility of rationally designing high surface area and porosity, would provide a large number of active sites for adsorption and catalysis. Besides its potential applications as a catalyst or catalyst support, biochar is being investigated and employed in advanced sorbents, fertilizers, *etc.* (Huang et al., 2016; Uzun et al., 2016).

The chemical nature of biochar can also be modified through post-treatment processes, such as acid washing or chemical activation. These processes can alter the surface chemistry and functional groups of biochar, resulting in enhanced adsorption capacity and improved performance in environmental applications. Besides more or less complex C-based structures, thermal treatments of biomass for biochar production, often

leaves K–Ca–Mg–Na carbonates, Ca–K–Mn silicates, K–Na–Ca chlorides, Ca–Al–Mn oxides, sulphates, and phosphates (Vassilev et al., 2014; Omoriyekomwan et al., 2021a; Vassilev et al., 2012), which content in the final biochar product can be adjusted via post-treatment processes.

The phenomena of mass transfer on the surface of biochar during heterogeneous catalysis can be divided into the following stages (Lee et al., 2017): a) diffusion of the reagent from bulk gas or liquid film to the external surface of the catalyst; b) diffusion of the reagent to the inner surface of the catalyst through the pores of the catalyst; c) adsorption of the reagent on the surface of the catalyst; d) reactions occurring on the catalytic active centres on the catalyst surface; e) desorption of product from the catalyst surface; f) diffusion of product to the internal surface of the catalyst through catalyst pores; g) diffusion of product from the external catalyst surface to bulk gas or liquid film (Lin and Huber, 2009). Thus, catalytic activity is highly contingent on accessibility to catalytic active sites dispersed throughout internal pores. Although biochar is a porous material, the morphology and porosity of biochar without activation demonstrates poor catalytic properties. Various pretreatments can be applied to modify biochar morphology and porosity, as highlighted in Section 2.3. Surface area, pore size, pore volume, pore type [i.e., micropores, mesopores and macropores (Bikbulatova et al., 2017)] are vital properties, that impact overall catalytic ability.

Despite discussed benefits, the effective conversion of biomass into high-performing nanomaterials on a large scale for electrocatalytic purposes remains challenging (Alston and Arnold, 2011; Sharma et al., 2011). Amongst the major technical barriers presenting significant challenges in terms of materials comparison or standardisation of production processes, we can mention the high water soluble fraction, the (already discussed) huge variability of organic compositions of different biomasses, and to some extent, the large variability of inorganic components too (Alston and Arnold, 2011; Sharma et al., 2011).

2.2.1 Thermochemical biomass-to-biochar conversion processes

As previously described, the solid material obtained from the thermochemical conversion of biomass in an oxygen-limited environment is referred to as biochar (Liu et al., 2015a). Biochar can be produced via *pyrolytic*, *hydrothermal*, *carbonization* and *graphitization* methods. Because biochar can be constituted by multifunctional CNs, the thermochemical conversion of biomass into biochar for catalytic purposes is regarded as a biomass upgrading process (Liu et al., 2015b).

Pyrolysis is one of the most developed process for the conversion of biomass into biochar and it is ordinarily carried out in the 400°C–700°C temperature range and in an inert environment. Compared to other thermochemical conversion methods, pyrolysis is characterised by generally higher heating rates when compared to other thermochemical processes, benefitting the production of gaseous and liquid phases (Shafizadeh, 1982; Liu et al., 2015b). Pyrolytic processes are ordinarily performed via either conventional or microwave heating. From a structure perspective, pyrolytic biochar products are mainly constituted of amorphous carbon phases with low degree of crystallinity, specific surface, and porosity (Jatav et al., 2017).

Hydrothermal carbonisation (HTC) treatments operating at relatively low-temperature ranges, of about 170°C–250°C, and over a period of time ranging from a few hours to a day, offer significant advantages for biochar production, including a much reduced energy requirements for temperature; post thermal treatment drying processes; and enhanced compatibility with high water levels in the biomass feedstocks (Sch et al., 2011). HTC biochar is usually constituted by carbonaceous species with a high level of O-doping and/or a large amount of oxygen-containing functional groups, and generally high oxygen content. Depending on the final application and/or targeted properties/characteristics of the CNs catalyst, further treatments and modifications might be necessary, especially if O-free catalysts are desired.

Carbonization of biomass can generate a carbonaceous framework at a higher (compare to pyrolysis) temperature range, and in general between 700oCand 900°C (Liu et al., 2015b). Volatile components present in the source biomass are removed up to 95% at these temperatures, resulting in the formation of hierarchically porous carbons (HPCs). HPCs exhibit high specific surface areas (<1,000 $m^2 g^{-1}$) and large pore volumes (<1.5 $cm^3 g^{-1}$). HPCs show great application potential as catalyst supports for fuel cells and supercapacitors (Zhang L.-L. et al., 2023).

Graphitization is a thermal treatment of carbonaceous materials at temperatures ordinarily in the range 900oC–1800°C, or higher, in an inert atmosphere. Graphitization is a process that converts low-ordered amorphous-like carbonaceous layers or turbostratic carbon into highly ordered structures (Andrews et al., 2001). Graphitization is usually a further step in the production of highly ordered nanostructured biochar produced via pyrolysis or carbonization, useful for tuning structural as well as electronic properties (Thompson et al., 2015).

2.2.2 Temperature dependent types of biochar and main nanostructured features

The use of hydrocarbon-rich organic waste has made significant progress in the growth of CNs leading to promising paths for their commerzialization (Wang et al., 2018; Omoriyekomwan et al., 2021b). Volatile compounds, such as alcohols, phenols, CO, and hydrocarbons derived from biomass (Shen et al., 2011; Omoriyekomwan et al., 2016) are critical carbon sources for the production of CNs by chemical vapor deposition (CVD) process (Kuznetsov et al., 2001; Maruyama et al., 2002; Zhao et al., 2006). It has been investigated that biomass undergoes a physical-chemical transition process as charring temperature increases from 300oC to 700°C (Keiluweit et al., 2010). Four types of biochars encompass a distinct mixture of physical and chemical phases: 1) Amorphous biochars characaterised by a random mixture between heat-altered molecules and incipient aromatic polycondensates; 2) Transition biochars where the crystalline character of the precursor is preserved; 3) Composite biochars comprising graphene stacks which are poorly ordered and embedded in amorphous phases; 4) Turbostratic biochars characterised by disordered graphitic crystallites (Keiluweit et al., 2010). Concurrently, when metals such a Fe and Mg are involved in the carbonization of biomass, biochar with a high occurrence of aromatic compounds was reported (Zhang et al., 2013).

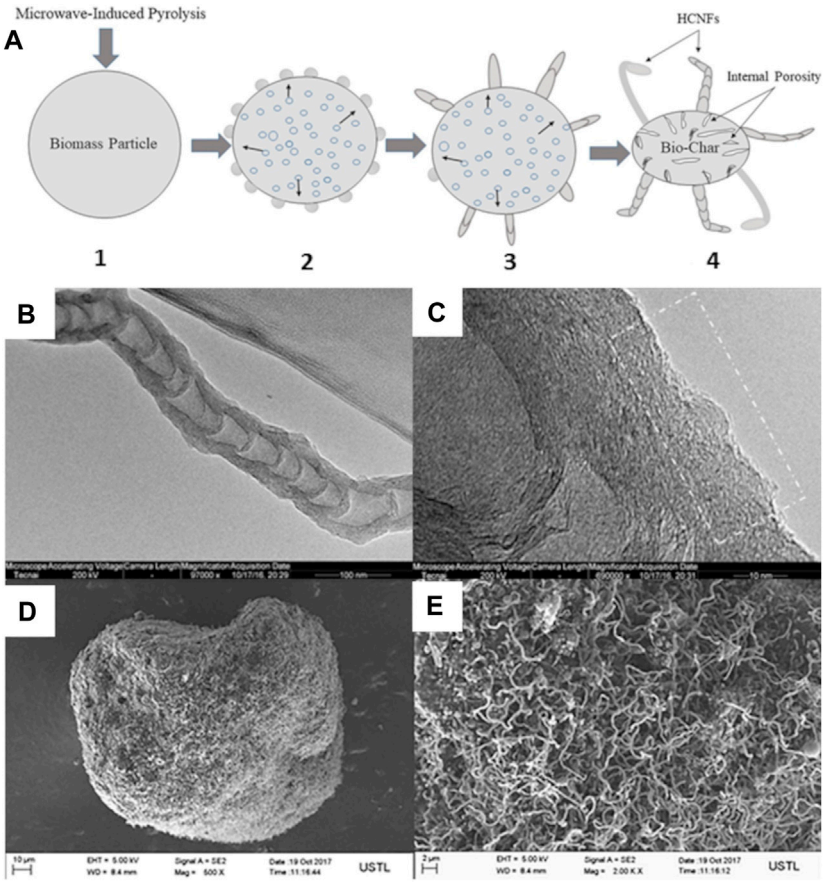

FIGURE 2
(A) Self-extrusion mechanism of the growth steps of HCNFs: (1) microwave-induced pyrolysis of biomass; (2) self-extrusion of volatiles from inside of the biomass particle through pores on biomass surface and resolidification of volatiles on the particle surface, initiating the HCNFs formation; (3) continuous volatiles through nano-sized channels, initiating the growth of the HCNFs; (4) growth of HCNFs on porous bio-char; **(B)** TEM and **(C)** HRTEM images of HCNFs on microwave pyrolytic PKS biochar at 600°C (Omoriyekomwan et al., 2017). **(D, E)** SEM images of bio-chars obtained during microwave pyrolysis of isolated cellulose from PKS components via the alkali-acid method at 600°C (Omoriyekomwan et al., 2019). Reproduced and modified with permission.

There has been extensive research in fabrication of CNs such as CNTs/CNFs, nanoribbons, graphene, fullerenes, via biomass as a low cost and green carbon source (Shi et al., 2014; Omoriyekomwan et al., 2017; Sun et al., 2018; Omoriyekomwan et al., 2019). Generally, all CNs can be divided into: a) zero-dimensional (0D) quantum dots, fullerenes, nanosphere, core@shell, yoke@shell; b) one-dimensional (1D) nanorods, nanowires, CNTs, CNFs; c) two-dimensional (2D) nanosheets, graphene, nanoplates, nanobelts; d) three-dimensional (3D) hierarchical mesoporous nanostructured assembly, metal organic frameworks (MOFs). The properties of 0D/1D/2D/3D CNs can vary in mechanical strength, surface area, hydrophobic adsorption, scarcity, *etc.* The mechanism of biochar network formation divided into the main crucial steps (decomposition, rapid volatilization, polymerization-depolymerization, dehydration, intramolecular rearrangement, intramolecular condensation and aromatization). The biochar network obtained from various biomass can be transformed into more ordered graphitic nanostructures involving dehydration, decarboxylation, rearrangements, aromatization, and intramolecular condensation to form 0D, 1D, 2D nanostructures or it can be converted to the low molecular 3D carbon nanomaterials.

2.3 Biomass pretreatment methods

Chemical pretreatment of biomass is often regarded as a strategy to impart a particular porosity, microstructure and/or morphology to the final CNs. Omoriyekomwan et al. (Omoriyekomwan et al., 2017) compared microwave-assisted and conventional (fixed-bed) of raw palm kernel shell (PKS) pyrolysis approaches. Hollow carbon nanofibers (HCNFs) were successfully produced on the surface of bio-chars during microwave pyrolysis of PKS at 500 °C and 600°C. The observed HCNFs onto the PKS biochar was attributed to the microwave heating condition only and not detected under conventional heating. Authors explained this phenomenon by the difference in heat transfer mechanism in microwave and conventional heating. The yield of observed hollow carbon nanofibers (HCNFs) increased with temperature and reached 9.88 wt% at 600°C (Omoriyekomwan et al., 2017). A self-extrusion mechanism of volatiles from inside of the biomass particle through pores on biomass surface and resolidification of volatiles on particle surface bio-component was attributed for CNTs formation under microwave irradiation at 600°C (Figure 2). Additionally, the presence of Fe, K, and Ca in raw PKS biomass

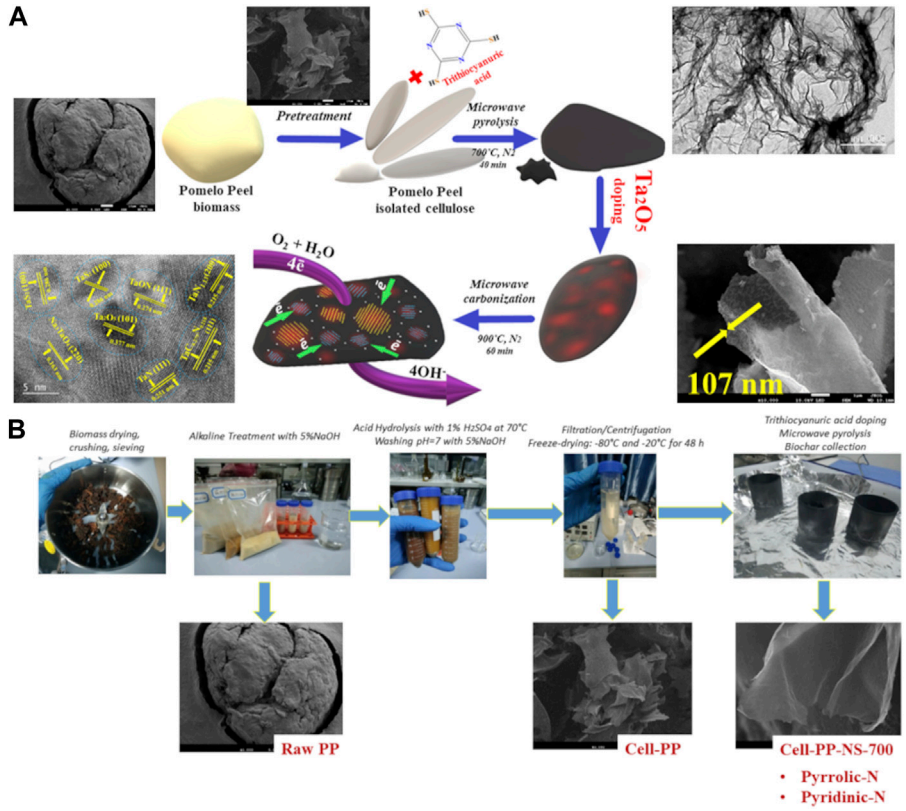

FIGURE 3
(A) Schematic diagram introducing the evolution of carbonaceous nanostructure during the pretreatment of biomass and pyrolysis process and **(B)** the detailed synthesis route of the N, S, Ta-doped carbon nanosheets. Reproduced and modified with permission (Maliutina et al., 2021b).

and in the HCNFs structure was considered to have an important role during their formation and growth (Omoriyekomwan et al., 2017).

In another study of Omoriyekomwan et al. (Omoriyekomwan et al., 2019), microwave pyrolysis for 1 h at 600°C was carried out on the raw PKS (Figures 2B, C) and isolated cellulose without addition of external catalyst (Figures 2D, E). Two different pretreatment methods, i.e., alkali-acid and formic acid/acetic acid were systematically compared. The higher yield of formed CNTs was correlated with the two-step alkali-acid (NaOH for lignin isolation/ H_2SO_4 for cellulose isolation) route of the raw PKS biomass (Omoriyekomwan et al., 2019). The chemical alkali-acid pretreatment displayed effective synthesis of CNTs that greatly enhanced their length (600–1800 nm in this study vs 200–1,600 nm of commercial CNTs) (Figure 2E) (Omoriyekomwan et al., 2019). The observed Raman I_D/I_G ratio for CNTs synthesised in this study was lower (0.86) compared to that of commercial CNTs (0.96) was attributed to lower amount of defects and higher order of the nanostructure, resulting in higher quality (Omoriyekomwan et al., 2019).

Recently, Maliutina et al. (Maliutina et al., 2021b) reported two-step chemical pretreatment and pyrolysis methods that were employed to pomelo peel biomass to obtain mesoporous carbon nanosheets (Maliutina et al., 2021b). The formation of carbon nanosheets with a thickness of about 107 nm (Figure 3A) was obtained from irregularly shaped pomelo peel as a precursor using a chemical pretreatment process, involving alkaline etching with KOH and acid hydrolysis with H_2SO_4 (Figure 3B). The final cell-PP-NS-700-Ta-900 nanosheet sample also exhibited a moderate graphitization degree (ID_1/IG ratio of 1.11) and high specific surface area (SSA) of 336.82 $m^2\ g^{-1}$. This chemical pretreatment method was regarded as a promising route for fast and tunable conversion of the complex pristine biomass microstructure into a nano framework with desirable properties.

Cyclic oxidation pretreatment of biomass for CNs synthesis has been reported in other works (Kang et al., 2005; Goodell et al., 2008). The cyclic oxidation process allows for the conversion of biomass into tubular carbon nanostructure via a repetitive (i.e., cyclic) oxidation process. Goodell et al. (Goodell et al., 2008) used six different feedstock, including wood fibers, avicel cellulose, bamboo, alpha-cellulose, organosolv lignin, and wood fibers. All samples were preheated before cyclic oxidation at 240°C and 400°C, respectively. They reported hard tubular CNTs formation in cellulose samples, organosolv lignin, and filter paper. It was concluded that the original biomass structure played an essential role in the formation of CNs via the cyclic oxidation method.

The Authors proposed a nanoscale channel formed at low-temperature carbonization treatment that acted as the templates for the CNTs' growth (Goodell et al., 2008). The formation of nano-channels at low-temperature carbonization promoted cellulose ablation, which contributed to CNTs synthesis. Nevertheless, when pure biomass components (such as lignin and cellulose) were subjected to cyclic oxidation, tubular CNTs were not formed.

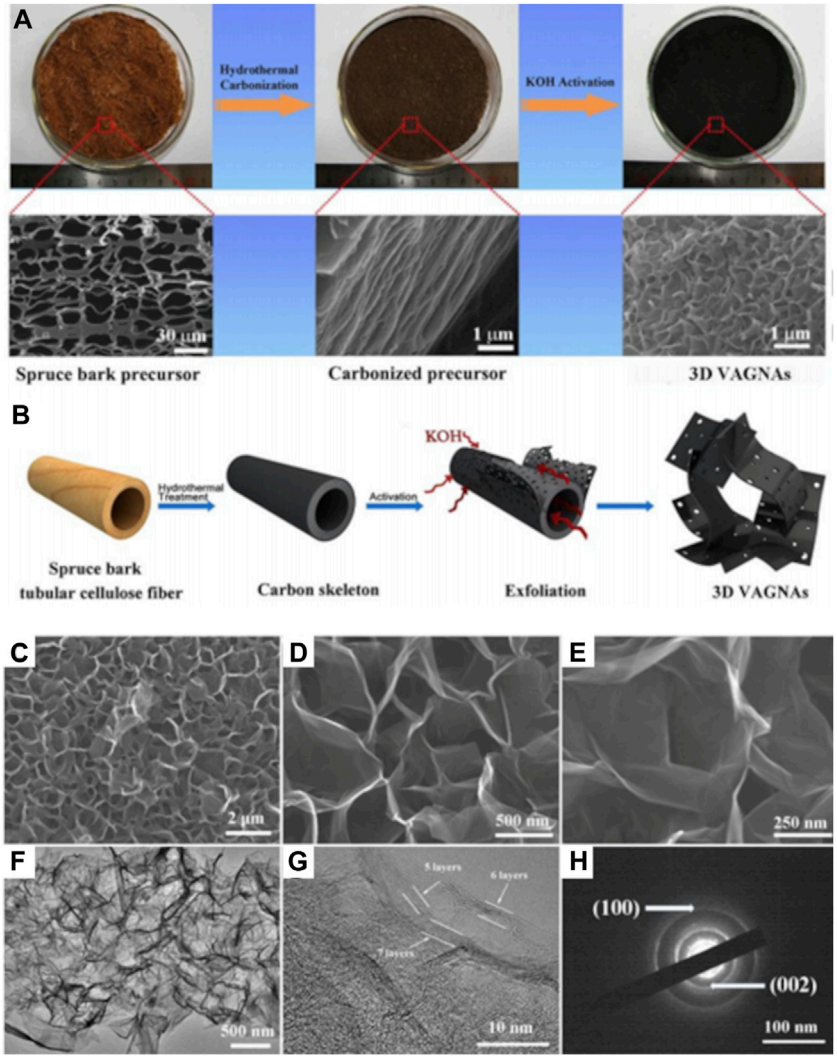

FIGURE 4
Schematic illustrations of carbonization and chemical activation treatment process **(A)** overall formation process and **(B)** the synthetic mechanism of 3D the vertically aligned graphene nanosheets (VAGNAs); **(C)** SEM image of the microstructures of VAGNA-900; **(D, E)** High magnification SEM pictures showing the vertically aligned graphene nanosheets of VAGNA-900; **(F)** TEM image of VAGNA-900; **(G)** HR-TEM image of VAGNA-900 demonstrating its few-layer feature; **(H)** SAED image of VAGNA-900. Reproduced and modified with permission (Sun et al., 2018).

Mechanical activation treatment was proposed by Chen et al. (Chen and Chadderton, 2004) when they reported the synthesis of aligned CNTs from iron phthalocyanine pyrolysis after ball milling treatment. Milling time was observed to be the most important controlling parameter in this process (Chen and Yu, 2005; Onishchenko et al., 2012; Onishchenko et al., 2013a). Onishchenko et al. (Onishchenko et al., 2013b) reported the formation of CNTs from sphagnum moss and agricultural wastes via a mechanical activation process. The CNTs content after mechanical activation was 11.52 wt%, 24.45 wt%, 34.06 wt%, and 42.75 wt% for mechanical pretreatment duration of 7, 10, 16, and 27 h, respectively (Onishchenko et al., 2013b). It was observed that after 10 h of mechanical treatment, most of the materials were enriched with CNTs. In other study of Reva et al. (Reva et al., 2016a), abundant CNTs were presented in all bulk material derived from brown sphagnum moss biomass after 36 h treatment. Electrostatic interaction of the CNs was reported to be responsible for the felt-like aggregates forming with a size of 20–100 μm, consisting of CNTs and amorphous carbon (Reva et al., 2016a; Reva et al., 2016b). It is worth noting that there was no catalyst involved in synthesizing CNs from biomass using mechanical treatment, while amorphous carbons acting as the precursor of CNs before mechanical activation were readily obtained from biomass. Therefore, mechanical pretreatment is a favorable technique for the synthesis of CNs as a result of the low cost of technology and feedstock.

H_3PO_4, and $ZnCl_2$ are also used alongside KOH as pretreatment agents prior to pyrolysis (Chaparro-Garnica et al., 2021). This method has showed to enhance porosity and ensurehigh specific surface area (SSA) of the final CNs (Chen et al., 2016). Li et al. pretreated willow catkin in KOH aqueous solution based on a mass ratio of 1:1 and obtained an interconnected porous carbon nanosheet after pyrolysis (Li et al., 2016). Meanwhile, large SSA of 2,385 m^2g^{-1}, a large pore volume, and easily accessible open

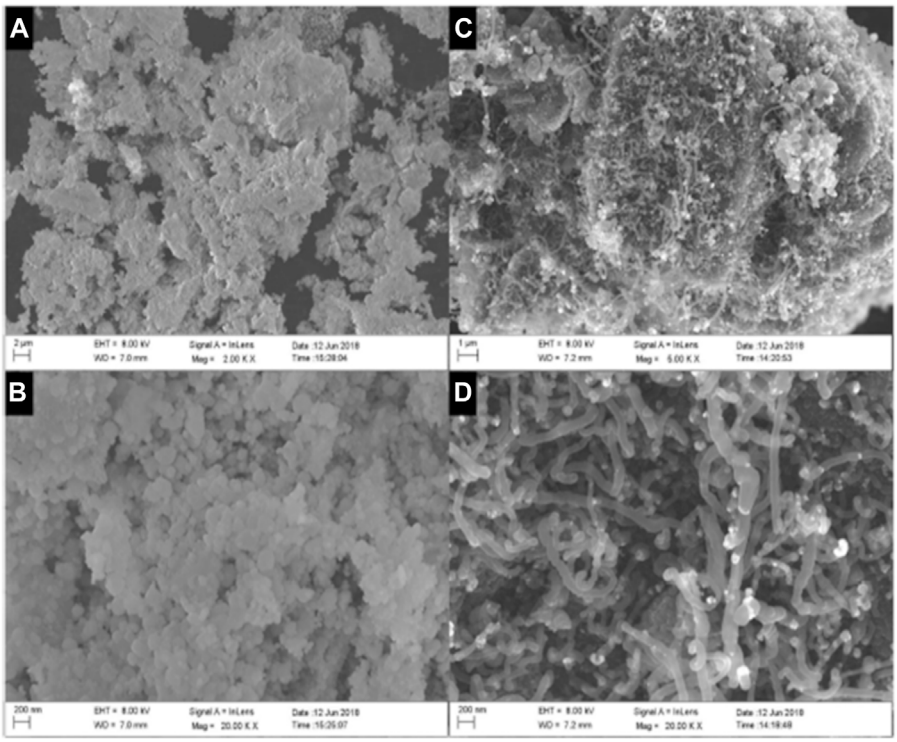

FIGURE 5
SEM images of biochar-NiO and biochar-CNT-NiO: **(A)** and **(B)** different magnifications of biochar-NiO; **(C, D)** different magnifications of biochar-CNT-NiO. Reproduced with permission (Zhang et al., 2021).

surfaces of graphene nanosheets were achieved from spruce bark after HTC at 180°C and KOH pretreatment (Figures 4A–H) (Sun et al., 2018). Chemical pretreatments of biomass were also proven to be beneficial in the case of biochar synthesis from graphitisation processes (Sun et al., 2013; Mahmoudian et al., 2016; Su et al., 2017). Interesting observations were also reported in the case of chemical pretreatment prior pyrolytic biochar synthesis via microwave heating rather than conventional heating. Zhang et al. (Zhang et al., 2021) synthesized biochar-CNTs composite from char from pine nutshell char via microwave heating (Figures 5A–D).

The Authors impregnated the source biomass with Ni catalyst and applied microwave heating in an inert environment of CH_4/N_2 gas (60/40 vol%) for 20 min reaching 600°C. Enhanced CNTs growth was reported and ascribed to the conversion of Ni nanoparticles into highly-crystallized NiO nanoparticles (Zhang et al., 2021). Supplementary Table S2 summarises biomass-based CNs obtained from different pretreatment and fabrication methods that were examined by this review.

It can be seen in Supplementary Table S2, that the preferable temperature range to produce CNTs enriched biochar is 700°C–800°C, while production of carbon nanosheets correlates with the range of 700°C–900°C. It is worth to note, that the microwave pyrolysis method assists to produce CNTs at the lower temperature range of 600°C–700°C. It can be explained by the difference in heat transfer mechanism in microwave and conventional heating. Unlike conventional heating, during microwave irradiation the particle temperature is higher than the surrounding area due to the selective heating under microwave. During microwave pyrolysis, the released volatiles are extruded through pores on biomass particle surface. Upon release, the high molecular weight tar precursors solidify due to lower temperatures at particle surface compared to particle core, initiating CNTs/CNFs formation and growth via CVD mechanism. Graphene nanosheets can be obtained at temperatures above 850°C during the graphitisation process, but requires a catalyst, such as Fe or Zn based.

3 Electrocatalysis of biomass-derived nanostructures

As already mentioned, one of the major drive for the use of biomass-derived nanostructured electrocatalysts remains the replacement of precious and rare metals in electrocatalytic processes. This can open up exciting new opportunities for very large scale deployment of electrocatalytic processes (i.e., electrolytic water splitting for hydrogen generation), that are sustainable, circular in their economy, and significantly cheap than current processes based on platinum group metals. In order to achieve this, major techno-scientific barriers such as the general low efficiencies of biomass-derived electrocatalysts (Seh et al., 2017), when compared to their precious metal-based counterparts, need to be overcome. In this review, we focus our attention on recent advancements reported in the field of biomass-derived electrocatalysts for hydrogen evolution and oxygen reduction/evolution, at the heart of water splitting, fuel cells and metal-air

batteries (Martín and Pérez-Ramírez, 2019) technologies, that urgently require alternatives to currently used platinum group metal-based electrocatalysts. A true rational design of novel C-based, sustainable, electrocatalysts can only be achieved through creating and controlling active sites, in conjunction with an in-depth understanding of electrocatalytic reaction mechanisms and kinetics. With the intent of promoting and encouraging such an approach, this review will try to develop a framework for rationalising activity trends and guiding electrocatalyst design contextualising recent results and observations on the basis of a combination of materials science, computational science, and inorganic chemistry (Hwang et al., 2017).

3.1 Benchmarks for biomass-derived electrocatalyst for ORR/OER/HER and targeted structural attributes

As an alternative to precious metal-based catalysts, various CNs, such as CNTs/CNFs (Wu Z.-Y. et al., 2018), and graphene-based nanosheets (Gong et al., 2019; Tang and Qiao, 2019) have been reported as ORR/OER electrocatalysts. CNs are generally functionalized via doping, allowing to generate functionalised electrocatalysts with a superior electrocatalytic activity (Zhang et al., 2016b). Dopants alter the amount of crystal and surface defects acting as potential catalytic active sites and modify the electronic structure of the CNs (Zheng et al., 2014; Wu et al., 2017), with a direct influence on the thermodynamics and charge carrier distribution in the carbon-based electrocatalysts (Sharifi et al., 2012; Lu et al., 2017; Mamtani et al., 2018; Jiang et al., 2019b). Typical types of doping include mono/dual/multiple heteroatoms doping; defective/vacancy doping; and charge-transfer doping.

Doping of graphene frameworks with non-metal elements such as N or O has been reported as a convenient strategy to tune the electrochemical as well as optical properties of graphene nanostructures (Inagaki et al., 2018). Zhang L. et al. (Zhang and Xia, 2011) investigated the role of nitrogen heteroatom towards ORR based on density functional theory (DFT) calculations applied to a N-doped nanographene model ($C_{45}NH_{20}$) in acidic medium. Nitrogen doping introduces an unpaired electron (the latter causing localized distribution of the molecule orbitals) with the overall result of enhancing the chemical reactivity of the graphene itself. Their simulations demonstrated that ORR on N-doped graphene is a direct four electron pathway, and consistent with experimental observations. Interestingly, the Authors identified the active catalytic sites on single nitrogen doped graphene, having either high positive spin density or high positive atomic charge density. N doping introduces asymmetry spin density and atomic charge density, allowing for N-graphene to exhibit high electroncatalytic activities for the ORR (Zhang and Xia, 2011). The electrocatalytic performance of the heteroatom-doped CNs partially depends on the electronic structure of the heteroatoms in comparison to the positively charged C atoms. In this case, the selectivity of a specific reduced product strongly depends on the affinity of active sites towards the corresponding intermediate motifs. This is quite different from the conventional pristine CNs.

Experimentally, different N functionalities in the carbonaceous skeleton can be easily probed and interrogated via X-Ray photoelectron spectroscopy (XPS) given the distinguishable N 1s binding energy of pyridinic-N (ca. 398 eV), pyrrolic-N (399–400 eV), graphitic-N or quaternary-N (ca. 401 eV), and pyridinic N oxide (402–406 eV) (Maliutina et al., 2018; Jiang et al., 2019a; Maliutina et al., 2021b). Pyridinic-N exists on the edge of the graphene layer and bonds to two carbon atoms, containing a lone electron pair, which can boost the electron-donor capability of the carbon material, resulting in the improvement of the adsorption capacity of O_2 and onset potential for ORR (Lai et al., 2012). Whilst incorporated into the graphene layer and bonded to surrounding three carbon atoms, graphitic-N donates one extra electron to the carbonaceous skeleton that weaken the O-O bonds and decrease the energy barrier for the first electron transfer (rate-determining step). Overall, graphitic-N functionalities facilitate the limiting current density and electron transfer for ORR. Wang and co-workers (Wang D.-W. et al., 2012) postulated that pyridinic-N and pyrrolic-N improve the storage of hydrogen atoms and accelerate protonation. At the same time, the oxidized-N functionalities exhibit a high affinity to electrons, unlike less positively charged pyridinic-N. The edge plane graphitic-N (valley) acts the same as pyridinic-N centers via a four-electron pathway, while graphitic-N (center) acts via a two-electron pathway, as elucidated by Sharifi and co-authors (Sharifi et al., 2012). Xing and co-authors postulated that the pyridinic-N form and the neighboring carbon atom play a crucial role in ORR activity (Xing et al., 2014). The ORR and OER activity was observed to increase with an increase in pyridinic-N site density. Mamtani and co-workers postulated the correlation between higher content of the pyridinic-N active site and electrocatalytic activity towards both ORR and OER (Mamtani et al., 2018). Notwithstanding, the research community still debates what form of nitrogen, pyridinic-N, graphitic-N, or their particular ratio make a more significant contribution to electrochemical performance based on both computational and empiric features (Matter et al., 2006; Guo et al., 2016; Singh et al., 2019).

Incorporation of the elements from the second row of the Periodic Table with a larger radius than carbon leads to significant distortion of planar structures creating defects that act as active centers towards ORR/OER as well as HER. S-doping can effectively alter spin/charge density distribution and distorts the carbon lattice by creating large electroactive sites. Sulfur doping was observed to alter spin density distribution via formation of several different sulfur-containing functionalities, including thiophene (aromatic sulfur), thiol, thioesters, sulfoxide, sulfone, and sulfonic acid (Zhao et al., 2012).

XPS showed that a series of four major peaks (S 2p peaks appear as doublets of 2p3/2 and S 2p1/2 due to spin-orbit splitting) can be expected in the C lattice; i.e., at binding energies of 163.80 eV and 165.20 eV corresponding to the S 2p3/2 and S 2p1/2 peaks of the C–S–C bonds, and at binding energies of 167.7 eV and 169.3 eV corresponding to S 2p3/2 and S 2p1/2 indicative of C–SOx–C species, where x is 2, 3, and 4, respectively. (Wang Z. et al., 2014; Zhang J. et al., 2020; Maliutina et al., 2021b). Furthermore, the doping of carbon framework with phosphorous introduces reduced unstable P–O groups as phosphate, phosphine oxide, phosphonic acid, and substituted C-P-C phosphine, thereby improving the electrochemical properties. The XPS P *2p* spectra of carbonaceous metal-free materials exhibit a predominant P–C

characteristic peak and P–O bond at 131.0 ±0.7 eV and 133.7 ± 0.5 eV (Huang et al., 2018). In particular, it has been reported that the co-doping of CNs with two [such as N/S (Wang X. et al., 2014; Ito et al., 2015), N/P (Borghei et al., 2017; Cheng et al., 2021), or N/F (Akula et al., 2021)] or even multi-doping [such as N, S, P and F (Liu et al., 2016; Huang et al., 2018; Li Y. et al., 2019)] with several heteroatoms is an effective way to boost their electrochemical activity synergistically. Recently, Li et al. reported no synergetic effect between N and S dual-doping towards ORR, while the sequence of doped heteroatoms played a critical role (Li J.-C. et al., 2019). Due to this phenomenon, doping of S followed by doping of N promotes the formation of pyridinic-N functionalities. This is attributed as the most active functional group in N, S dual-doped electrocatalyst towards the ORR, while on the counter doping of N followed by doping of S reduces the content of pyridinic-N species, which leads to a nadir of ORR performance (Li J.-C. et al., 2019).

For oxygen adsorption, only the sample with pyridinic-N functionalities possesses binding energy of −1.4 eV, which is superior to that of pyridinic-N-S (−1.0 eV), graphitic N (−1.1 eV), and graphitic-N-S (−1.0 eV) (Li J.-C. et al., 2019). Additionally, the Gibbs free energy diagrams for different catalyst models in an alkaline environment were presented by authors (Li J.-C. et al., 2019) observed all the reaction intermediates (O_2*, OOH*, O* and OH*) formed during ORR. Pyridinic N (green line) plentifully contributes the ORR *via* the OOH* formation with a small energy barrier (0.3 eV), as well as the fact that only the pyridinic N can chemically adsorb O_2 that overall contribute to the ORR. Pyridinic-N functionality was also mentioned as the major responsible active site in other valuable studies (Rao et al., 2010; Zhang and Xia, 2011; Vikkisk et al., 2014; Xing et al., 2014). Notwithstanding, it is still difficult to distinguish the role of secondary or especially tertiary doped heteroatoms not only by computational DTF simulations but especially for such a complex biomass-derived carbonaceous matrix both experientially and theoretically.

The synergy between various techniques can avoid, to a great extent, the limitations of using one sole technique. For example, the advances in using a combination of *operando* XRD and Raman spectroscopy are desired, which enables the complementary characterisation of nanocatalysts in both surface and bulk levels (Zhang H. et al., 2023). Under *operando* conditions, the adsorbate and intermediate species, as well as the structural parameters of the catalyst can be simultaneously traced for an extensive understanding of the reaction pathways and elucidate the role of active centres. Structural defects, such as vacancies, substitutional or interstitial impurities, are regions of absorptive binding for gases and ions are successfully examined by scanning tunnelling microscopy (STM) (Feng et al., 2018; Xiao et al., 2021). X-ray absorption spectroscopy (XAS) has become a universal and in-depth characterisation technique that has been widely used in many fields due to the rapid development of synchrotron radiation sources. (Gao et al., 2017). Because of the difference in the relative absorption threshold of energy, the XAS can be divided into two parts: XANES (X-ray absorption near-edge structure, approximately 40 eV and below) and EXAFS (extended X-ray absorption fine structure, beyond the XANES region) (Xiao et al., 2017). The XAS analysis provides a myriad of information about the structure CNs and their dopants, such as the structure symmetries, element valence, bond distance and adjacent coordination environment of the atom (Liu et al., 2017). Although tremendous amount of works has described *in-situ* electrocatalytic characterisation, *in-situ* and operando characterization techniques and devices with a high resolution are necessary to elucidate the mechanism of defects due to the complexity of electrochemical reactions and the variety of imperfections. Consequently, the synergetic studies based on models of biomass compounds and comprehensive studies on *in situ* tunable engineering and activity of heteroatom-based active sites are highly desired for carbon-based electrocatalysts and a sustainable future.

3.2 Single doped biomass-derived nanocatalysts

Up to date, there are tons of works that report N-doped electrocatalysts towards ORR and a major part is belongs to alkaline electrolyte catalysis. Predominantly, their catalytic performance is still far from that of the Pt/C benchmark, although the characterization of nanomaterials very often describes similar nitrogenized functionalities and analogous distributions (Supplementary Table S3). Rationally incorporating one specific type of heteroatom for designing catalytic active sites remains one of the major challenges when thermochemically valorising biomass for production of efficient electrocatalysts for water splitting.

Zheng and co-authors derived a nitrogen self-doped carbon hollow cubes (NCHCs) was derived from L-lysine precursor at 1,000°C (Zheng et al., 2017). When used as electrocatalysts for the ORR, this composite exhibited an onset potential of 0.92 V vs RHE. This corresponds to a cathodic shift of only 61 mV of the half-wave potential of NCHCs when compared to that of commercial Pt/C (20 wt%), i.e., a common and widely used benchmark for ORR. Interestingly, the NCHCs composite also showed activity for the OER statistically comparable to another widely used commercially available OER standard, i.e., RuO_2/C (20 wt%). The E_{onset} potential close of that of Pt/C was attributed to the role of pyridinic-N and graphitic-N active structures. Wang and others used chitin biomass to fabricate N-doped 3D graphene-like nanosheets (N-DC/G) by doping with pretreating biomass with urea and proceeding with carbonization at 800°C (Wang et al., 2016).

The HRTEM image of the as-prepared N-DC/G sample displayed thickness of the layer less than 50 nm coupled with uniformly distributed porous structure. The corresponding K-L plots showed first-order kinetics towards ORR at different potentials and electron transfer number (n) of about 4, suggesting a direct four-electron pathway attributed to the presence of pyridinic-N and graphitic-N active sites. In another study, He and co-authors (He et al., 2019) used Taro stem plant biomass, impregnation with melamine, followed by KOH activation and carbonization at 800°C. The obtained biochar (3DNPC-800) displayed meso-/microporous 3D architecture with large SSA of 1,012 $m^2 g^{-1}$ and enriched nitrogen content, measured equal to 4.8 at %. The as-prepared biomass-derived 3DNPC-800 electrocatalyst exhibited ORR long-term stability (96.5% retention of the current density after 5.5 h) and resistance to methanol poisoning, which was attributed to the promoted formation of graphitic-N functionalities and developed 3D porous structure. Zhang and co-workers (Zhang

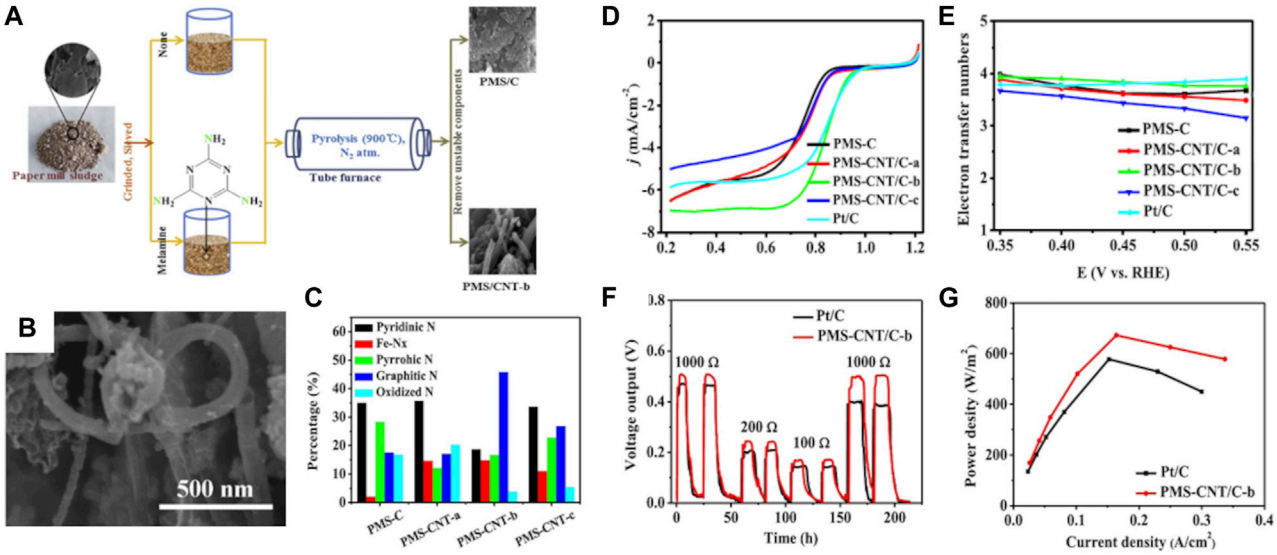

FIGURE 6
Illustration of the preparation process for the paper mill sludge-base catalysts of PMS-CNT/C-b sample **(A)**; SEM image of PMS-CNT/C-b sample **(B)**; nitrogen content as a function of differently prepared samples **(C)**; RDE curves of PMS-CNT/C-b sample at different rotation rates **(D)**; K-L plots at different potentials for PMS-CNT/C-b sample **(E)**; voltage outputs under three different loads **(F)** and polarization curves of Pt/C and PMS-CNT/C-b as the cathodes **(G)**. Reproduced and modified with permission (Zhang et al., 2019).

et al., 2019) synthesised N-doped CNTs from paper mill sludge (PMS) by treatment with melamine (PMS/CNTs-b) and carbonization at 900°C. Results are illustrated in Figures 6A–C.

The as-fabricated biochar displayed enriched formation of CNTs with predominant graphitic-N functionalities. The exceptional ORR activity of PMS/CNTs-b catalyst in contrast to that of Pt/C benchmark results in the most positive E_{onset} potential of 0.99 V vs RHE and current density of −6.96 mA cm^2 shown in Figure 6D. The calculated electron transfer number of the PMS/CNTs-b catalyst is a direct four-electron pathway, as can be seen in Figure 6E. The formation of CNTs was attributed to the addition of melamine, which was at first just considered as a nitrogen source to develop N-doped PMS-based catalysis in this work, during the pyrolysis of PMS. The remarkable ORR performance of PMS-CNT/C-b was correlated with the formed nanotube/nanoporous structure and the synergistic effect of abundant N groups, iron nitrides and thiophene-S. It can be seen in Figures 6F,G that the PMS/CNTs-b catalyst was employed in microbial fuel cells and possessed a power density of 675.72 W/m^2 that is improved when compared to Pt/C cathode (580.46 W/m^2).

A collection of biomass-based nanostructures with single heteroatom doping are reported in Supplementary Table S3 alongside physical chemical properties, and claimed active sites. From a comparison of the data reported in Supplementary Table S3 (as well as for most of the considered bifunctional or trifunctional electrocatalysts), graphitic-N was mentioned as the predominant active site.

3.2.1 Dual-doped biomass-derived nanocatalysts

The additional introduction of secondary heteroatoms, such as S, P, B and/or F into N-doped carbon is a promising strategy for boosting the electrochemical performance of carbon-based electrocatalysts (Xian et al., 2019; Zhang J. et al., 2020), although single S, P, B or F-doped biomass derived materials have shown electrocatalytic efficiency not as good as in the case of single N-doped. The complete picture explaining this enhancement effect promoted by the second dopant has yet to emerge, however, creation of catalytically active defects induced by the secondary heteroatom doping, as well as improvement of electronic properties of active site and surrounding which ultimately favour catalysis have both been proposed (Zhang et al., 2016c). In addition, the simultaneous presence of dopants and vacancies was observed to be more effective than doping alone, for example, in enhancing quantum capacitance as well as surface charge storage of graphene (Zhou et al., 2020).

Amiinu and co-workers synthesized N,S-codoped 3D assembled ultrathin graphene-like nanosheets (NSG) using cysteine as carbon precursor via thermochemical treatment at 900°C in the effort of developing bifunctional electrocatalysts for ORR/OER (Figure 7A) (Amiinu et al., 2016). Their graphene nanosheets exhibited mesoporous structure with BET SSA of 319.93 m^{2}g^{-1} and uniformly distributed heteroatoms (Figures 7B,C) with predominant graphitic-N, pyridinic-N, and thiophene-S species (Figures 7D,E). As shown in Figures 7F,G, the as-prepared graphene layers displayed comparable ORR performance to that of standard Pt/C electrode ($E_{1/2}$= −0.19 V and j_L= −5.34 mA cm^{-2} at −1.0 V) in an alkaline environment. Additionally, the NSG sample possessed promising OER activity and stability of 10 mA cm^{-2} at 0.69 V vs. SCE that is similar to that of IrO_2 (0.64 V vs. SCE) and a slight decrease of the oxidation potential only on 17 mV after the 1000th cycle, as shown in Figures 7H,I.

Han et al. (Han et al., 2020) proposed fructus azedarach biomass-derived N,P-codoped electrocatalyst (NPDC-1.09) as an

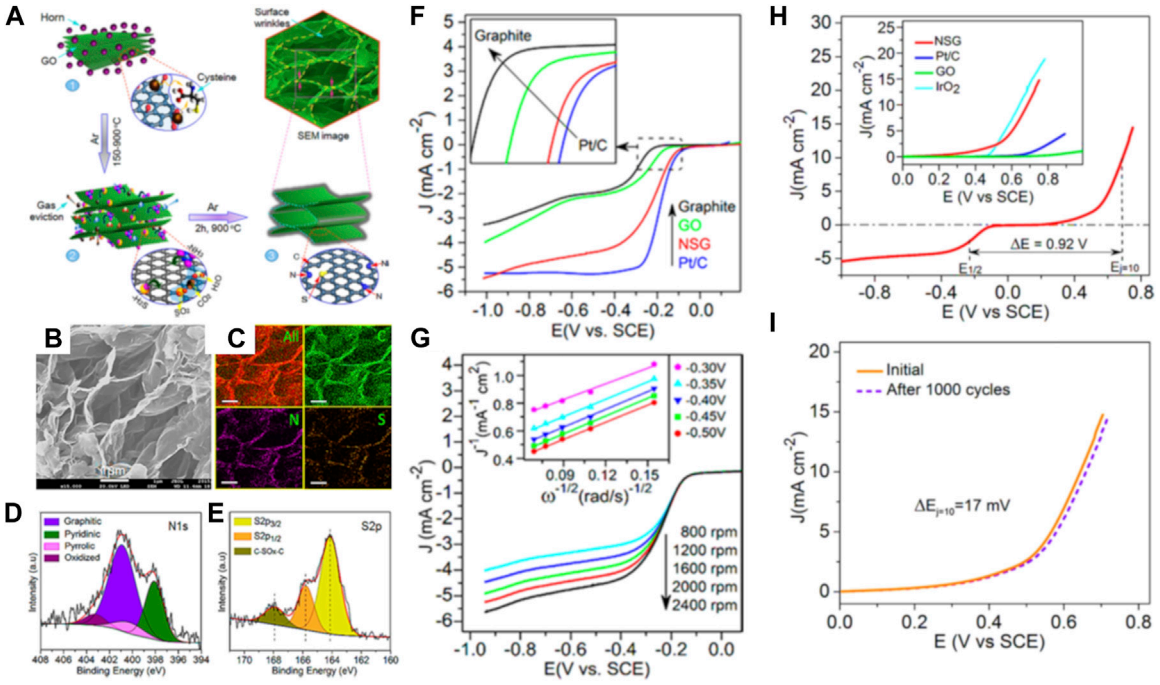

FIGURE 7
(A) Schematic illustration of the formation of NSG sample: (stage 1) Homogeneous mixture of graphene oxide and horn, (stage 2) disintegration/release of cysteine moieties and coverage of GO surface leading to the reaction of functional groups, eviction of gaseous species, and the formation of S and N containing moieties (e.g., H_2S, NH_3, *etc.*), and (stage 3) doping of N and S into the graphene carbon network;**(B)** FE-SEM image; **(C)** Elemental distribution EDX mapping of carbon, nitrogen and sulfur; **(D)** N 1s spectra and **(E)** S 2p spectra of NSG sample; **(F)** ORR LSV curves of graphite, GO, NSG, and Pt/C, and **(G)** ORR LSV at different rotation rates, Inset is the corresponding K-L plots; **(H)** Overall LSV potential curve of NSG sample (Inset is the comparison of OER currents of NSG, Pt/C, GO, and IrO2), **(I)** Stability of OER current before and after accelerated CV for 1,000 cycles. All data were recorded in 0.1 M KOH solution. Reproduced and modified with permission (Amiinu et al., 2016).

electrocatalyst for the ORR. TEM and HRTEM images show that the prepared NPDC-1.09 catalyst displayed a 3D porous nanosheet network with an interlayer spacing of 0.340 nm, indicating an amorphous structure with an I_D/I_G ratio of 1.09, suggesting a formation of numerous amount of defects due to N and P codoping. According to XPS characterization, nitrogen existed in pyridinic-N, pyrrolic-N, and graphitic-N forms, while phosphorous existed in P-O, P-N, and P-C moieties with an N: P ratio of 1.09 am %. Based on in-depth XPS and Raman observations, the theoretical structure of the carbon nanosheet of the NPDC-1.09 sample possible position of heteroatom defects in the carbonaceous backbone.

The electrocatalytic ORR activity was determined by LSV tests, where NPDC-1.09 catalyst exhibited E_{onset} potential of 0.94 V vs RHE and $E_{1/2}$ potential of 0.84 V vs RHE, and the potential gap of $E_{1/2}$ between Pt/C and NPDC-1.09 was 50 mV. The Tafel slopes of NPDC-1.09 and Pt/C reached close values of 119 and 120 mV dec^{-1}, respectively, suggesting promising activity towards ORR with reasonable kinetics for potential fuel cell applications. In other studies of Xiao and co-authors, phytic acid was used as a precursor to obtain N,P-codoped ultrathin nanosheets coated with multi-walled nanotubes at 900°C (CNT@NPC-900) (Xiao et al., 2019). The synthesized CNT@NPC-900 electrocatalyst displayed remarkable HER activities with overpotentials to reach a current density of 10 mA cm^{-2} of 167, 440, and 304 mV in acidic, neutral, and alkaline environments, respectively. Such promising activities were attributed to uniformly distributed N and P heteroatoms and formed pyridinic-N and P-O active sites. Additionally, the CNT@NPC-900 sample exhibited little degradation after 3000 CV cycles and supreme working efficiency for more than 100 h (Xiao et al., 2019).

Wang et al., 2017 employed guanidine carbonate salt as a biomass precursor to obtain B,N-codoped carbon nanosheets (BCN) to be tested for ORR (Figure 8A). Polyvinyl alcohol (PVA), boric acid, and guanidine carbonate molecules were used for cross-linking polymerization, then the gel precursor was pretreated with a symmetric triblock copolymer comprising polyethylene oxide and polypropylene oxide in an alternating linear fashion, PEO-PPO-PEO (Pluronic® P123), for the development of porous and nanosheet structure. After carbonization at 900°C in an N_2 environment, the gel precursor converted into 2D nanosheet layers architecture with uniformly distributed B and N heteroatoms (Figures 8A–C). Potential active sites were interrogated by XPS spectroscopy (Figures 8D–F), and it was found that boron formed B-N-C and B-O junctions whilst nitrogen showed the formation of C-N-B, pyridinic-N, pyrrolic-N, and graphitic-N functionalities. The SSA of 817 m^2 g^{-1} and an enriched porous structure were ascribed to the templating pretreatment with Pluronic® P123. It can be seen in Figure 8G that the BNC nanosheet sample possessed E_{onset} and $E_{1/2}$ values of 0.940 and 0.82 V vs. RHE, both of which are comparable to those of

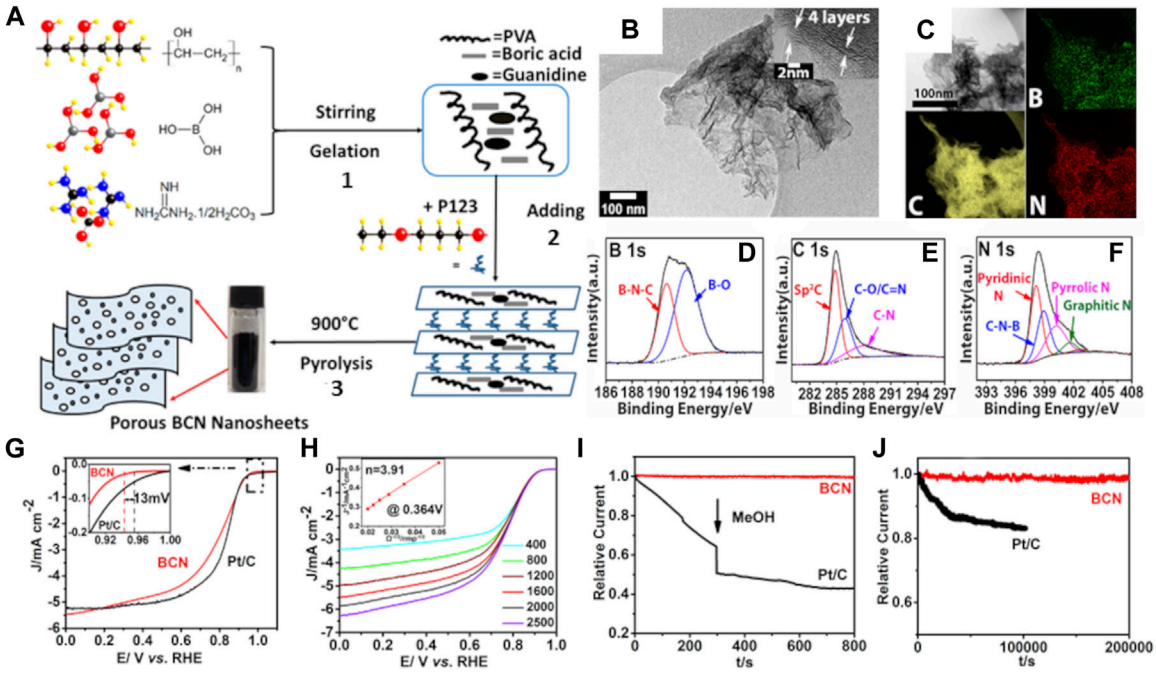

FIGURE 8
(A) The schematic synthesis process of porous BCN nanosheets including (1) Gelation of polymer precursor, (2) Addition of P123, and (3) Pyrolysis at 900°C under N_2; **(B)** TEM image of BCN nanosheet with 3–5 graphene layers; **(C)** TEM image of BCN nanosheets and corresponding EDS mapping of B, C, and N elements; XPS **(D)** B 1s, **(E)** C 1s, and **(F)** N 1s spectra of BCN nanosheets; **(G)** ORR catalytic performance of the porous few-layered BCN in 0.1 M KOH. LSV curves of BCN catalysts and Pt/C at a rotation rate of 1,600 rpm and a scan rate of 5 mV/s. The inset shows the higher magnification of LSV curves between 0.9 and 1.0 V vs. RHE; **(H)** LSV curves of BCN catalysts with various rotation rates from 400 to 2,500 rpm at a scan rate of 5 mV/s. The inset shows the corresponding Koutecky–Levich plot; **(I)** Chronoamperometric measurement for few-layered BCN and Pt/C in an O_2-saturated 0.1 M KOH solution and when 3.0 M methanol is added at around 300 s at an electrode rotation rate of 1,600 rpm; **(J)** Current-time chronoamperometric response of few-layered BCN and Pt/C in an O_2-saturated 0.1 M KOH solution at a rotation rate of 1,600 rpm. Reproduced with permission from (Wang et al., 2017).

Pt/C electrode, i.e., 0.953 and 0.84 V vs. RHE, respectively. The electrons transferred number is estimated to be 3.91 at 0.364 V vs. RHE derived from the Koutecky–Levich (K-L) plot and attributed to a four-electron pathway for ORR, as seen in Figure 8H. Finally, the BNC porous sample showed supreme crossover effect to methanol poisoning and outstanding long-time durability performance in alkaline medium (Figure 8J). Same remarkable that Pt/C ORR characteristics were reported in an acidic environment (Wang et al., 2017). Some of the outstanding codoped biomass-derived nanostructures towards electrocatalytic ORR/OER/HER are summarized in Supplementary Table S4.

3.2.2 Multi-doped biomass-derived nanocatalysts

One of the prospective ways to tune the photo-response property, generate higher electroconductivity, and facilitate the transport of the photoinduced charge carriers to the surfaces of the catalysts is the metal-free multidoping (i.e., three or even four heteroatoms simultaneously) due to diminished recombination of the electron-hole pairs with additional electrons. Non-metal multidoping strategies are yet to be fully understood and a significant amount of empiricism remains around multidoping in biomass-derived electrocatalysts, making any attempt at rational design very difficult (Wu et al., 2015; Zheng et al., 2016; Chang et al., 2020). Controversies also arise as to whether or not heteroatoms exhibit synergistic effects (Li Y. et al., 2019). The mechanism of multidoping and substitution is rather complex and thorough kinetic and mechanistic investigations need to be undertaken.

Huang and co-authors employed guanine as a precursor for the fabrication of N,S,P-multidoped nanosheets (GSP-1000) at 1,000°C (Huang et al., 2018).

The GSP-1000 sample exhibited ultrathin 2D carbon nanosheets and developed porous structure with uniform distribution of N, S, P, and O heteroatoms indicating sufficient development of defects in the carbonaceous matrix. XPS analysis indicated promoted the formation of graphitic-N, pyridinic-N, thiophene-S, and P-C defects. Rotating disk electrode (RDE) derived LSV ORR curve of GSP-1000 exhibited a comparable trend to that of commercial Pt/C activity with onset potentials (0.99 V vs RHE and 1.03 V vs RHE) and half-wave potentials (0.84 V vs RHE and 0.85 V vs RHE), respectively. The average electron transfer numbers derived from the linear Koutecky–Levich (K–L) plots demonstrated a favorable four-electron reduction pathway towards ORR. Good stability with the initial activity decreased only to 90.7% after a 4 h test and superior resistance to the methanol poisoning. In other study, authors also used guanine compounds to obtain similar to previous study 3D mesoporous graphene-like nanosheets (Huang et al., 2019). It was found that high temperature carbonization in the CO_2 environment leads to the controllable generation of mesopores and high SSA due to the etching effect of partial gasification reaction $C + CO_2 \rightarrow 2CO$.

TABLE 1 Summary of the multi-doped metal-free biochar-based electrocatalyst for ORR/HER/OER.

Pristine biomass	Obtained nanostructure	Approach	Synthesis method	Physical properties	Electrochemical properties	Active sites	Refs
Yeast and glucose	Yolk-shell	ORR	Pyrolysis at 800°C in N_2 for 2 h	SSA of 574.7 m^2 g^{-1} for mesopores and 580.6 m^2 g^{-1} for micropores; Structural defects (I_D/I_G = 1.25) due to the doping of N, P, and B	E_{onset}= 0.846 V vs RHE; 4e− pathway (n=3.78–3.90); Tafel slope of 72 mV dec^{-1} in O_2-sat. 0.1 M KOH; Good durability after 15,000 cycles	N/P/B-doping; Formation of N-B-C and B-N-C moieties; Doping of B attributed to boosting of ORR	Zheng et al. (2016)
Softwood kraft pulp	3D interconnected carbon nanofiber	HER	Solvothermal extraction of cellulose nanofibrils in tetrahydrofuran (THF) at 245°C/4.5 h; Pyrolysis with melamine and phytic acid at 400°C/2 h; Carbonization at 900°C/2 h	SSA of 682 m^2 g^{-1}; Structural defects (I_D/I_G = 0.88) due to the doping of N, P, and S	Tafel slope value of 99 mV dec^{-1}; An overpotential η_{10} of 331 mV vs. RHE in 0.5 M H_2SO_4	N/P/S-multidoping; predominant graphitic and pyridinic-N; thiophene-S	Mulyadi et al. (2017)
Guanine	Few-layered carbon nanosheets	ORR	Washing in H_2SO_4 and H_3PO_4 for 24 h; Pyrolysis at 1,000°C in N_2 for 1 h; Soaking in 1 M HCl for 10 h; Pyrolysis at 1,000°C in N_2 for 1 h	SSA of 486 m^2 g^{-1}	4e− pathway (n=3.8) in 0.1 M KOH; $E_{1/2}$ is 0.84 V $E_{1/2}$ is 0.67 V in 0.1 M $HClO_4$; $E_{1/2}$ is 0.70 V vs RHE in 0.1 M PBS	N//S/P-multidoping; pyridinic and graphitic N	Huang et al. (2018)
Spinach leaves	3D interconnected carbon nanosheets	ORR	Chemicsl activation with $ZnCl_2$ and carbonization at 850°C	numerous amount of defects (I_D/I_G = 1.17)	4e− pathway (n=3.81) in 0.1 M KOH; $E_{1/2}$=0.82 V vs commercial 20% Pt/C ($E_{1/2}$=0.86 V vs RHE)	N/S/P self-doping; pyridinic-N, pyrrolic-N, C-P, C-S-C, and C-N/P	Huang et al. (2020)

Lately, authors represented B,N,F-multidoped carbon nanosheets (BNFC-800) by using cigarette butts as biowaste precursors at 800°C (Zhang Q. et al., 2020). The as-prepared nanosheets possessed a mesoporous structure with uniformly distributed B, N and F heteroatoms. The XPS high-resolution spectra of B 1s heteroatom exhibited formation of B_4C, BC_3, BC_2O, B-N and BCO_2 functionalities indicating the sufficient substitution of carbon atoms at the edge by boron atoms and development of defective sites. Parallel, deconvolution of N1s spectra showed the formation of B-N, pyrrolic-N, pyridinic-N, graphitic-N and oxidized-N moieties, suggesting efficient incorporation of N heteroatom. The detected B-N bond (397.7 eV) displayed the interaction between B and N heteroatoms. F 1s spectrum consisted of ionic C-F (684.7 eV), C-F (687.8 eV) and semi-ionic C-F (690.4 eV) moieties. Authors attributed formed pyridinic-N, BC_3 and C-F species as active centers towards ORR and OER.

BNFC-800 sample possessed a Pt-like ORR activity with half-wave potential $E_{1/2}$ = 853 mV vs RHE. Following, OER activity was tested in 1 M KOH electrolyte. BNFC-800 showed a low overpotential of 313 mV to deliver 10 mA cm^{-2}, which was similar to IrO_2 benchmark. Furthermore, the as-prepared BNFC-800 electrocatalyst possessed a high battery performance of 51 mW cm^{-2} that is superior to Pt/C-IrO_2 with the maximum power density of 39 mW cm^{-2} (Zhang Q. et al., 2020).

Unfortunately, up to date, there is a lack of papers on metal-free multi-doped biomass-derived nanostructures towards ORR due to the complexity of controlling the formation of a desired structure from a given biomass or waste precursor (Table 1). Determining and rationally designing catalytic active centres and controlling surface engineering is far tougher than in the case of single-doped or dual-doped structures. To complicate this landscape is the lack of strong evidence on the synergistic effect of having multiple dopants and how (depending on their chemical nature) they interac with eachother and with the carbonaceous backbone.

3.3 Earth abundant metal-doped carbon nanostructures

Doping biomass derived carbonaceous nanostructured with Earth abundant, or not rare, metals can exploit the electrocatalytic properties of transition metals at relatively low costs, compositional flexibility, and provide opportunities for large scale production and deployment eliminating major barriers associated with the economy, origin, abundancy, production and supply chain typical of rare and precious metals (Han et al., 2019). Rationally designing earth-abundant hybrid electrocatalysts for ORR/HER/OER approaches as rare and precious metal substitutes is of extraordinarily importance in the quest to reach net zero carbon emissions. In order to enhance the electrocatalytic activity of carbonaceous catalysts and further extend their feasibility for electrochemical energy generation and storage devices, introducing certain TMs (Fe, Mn, Co, Ni, Cu, Mo, Ti, Ta, *etc.*) and their derivatives in form of oxides/suboxide, sulfides, selenides, nitrides/oxynitrides, carbonitrides is a sought after strategy. Previous studies indicate that adding iron (Wang K. et al., 2020) or cobalt

TABLE 2 Summary of the metal-doped biochar-based nanomaterials as electrocatalyst for ORR/HER/OER.

Pristine biomass	Obtained nanostructure	Approach	Synthesis method	Physical properties	Electrochemical properties	Active sites	Refs
Wine mash	Ultrathin nanoribbons	ORR	Pre-pyrolysis at 200°C in N_2 for 0.5 h; Washing in 3 M HCl; Carbonization at 850°C in N_2 for 1 h	SSA of 1,066.6 m^2 g^{-1}; Large structural defects, amorphous structure (I_D/I_G = 3.06) due to the doping of N and insufficient graphitization	4e− pathway (n=3.7) in 0.1 M KOH; $E_{1/2}$ is 0.84 V (vs RHE); Stability for 30,000 s maintains 90% of initial current	Metal-N (Fe-N); pyridinic-N	Wang et al. (2019)
Cellulose microfibrils	3D interconnected graphene nanosheets	ORR	Activation with KOH for 12 h and carbonization at 650°C 700°C for	Structural defects (I_D/I_G = 1.12) due to the doping of N	E_{onset}= 0.0 V vs Ag/AgCl; $E_{1/2}$= −0.15 V vs Ag/AgCl; 4e⁻ pathway (n=3.91)	Single atom (Fe); Fe-N; Pyridinic-N	Li et al. (2019d)
Spirulina microalgae	3D honeycomb-like nanosheet network with rough edges	ORR	Carbonization of spirulina at 800°C in N_2 for 2 h; Doping with g-C_3N_4 and urea; Carbonization of the mixture at 900°C in N_2	Ultralarge SSA of 1927.41 m^2 g^{-1}; Large structural defects, amorphous (I_D/I_G = 2.3) due to the doping of N and unsufficiemt graphitization	E_{onset}= 0.99 V vs RHE; $E_{1/2}$= 0.86 V vs RHE; 4e− pathway (n=3.87); Zn-Air Battery: OCV 1.44 V; P_{max} 179 mW cm^{-2}; the specifc capacity of 641.9 mA h g^{-1}; the energy density of 837.4 W h kg^{-1}	N content of 4.30 at%; S consists in pristine biomass; Single-atom (Fe) integrated with Fe_2O_3 clusters; Metal-N (Fe-N_x); C-S-C thiophene	Lei et al. (2020)
Vitamine B12	3D porous nanosheets	ORR/HER	Doping with g-C_3N_4; Pyrolysis at 500°C in N_2 for 2 h; Carbonization at 800°C in N_2 for 4 h; Washing in H_2SO_4 for 18 h	SSA of 634.9 m^2 g^{-1}; Structural defects (I_D/I_G = 0.94) due to the partial graphitization	ORR: $E_{1/2}$= 0.87 V vs RHE. HER: low overpotential (η_{10} = 319 mV). Zn-air battery: a peak power density of 101.3 mW cm^{-2} at a potential of 0.71 V	Co., N, P-doping; CoN_x-active sites	Niu et al. (2020)
Pomelo peel	Mesoporous carbon nanosheets	ORR	Pretreatment-KOH etching and H_2SO_4 hydrolysis; Isolation of cellulose nanofibers; Doping with trithiocyanuric acid and microwave pyrolysis at 700°C for 40 min; Microemulsion addition of Ta_2O_5 Carbonization in N_2 for 40 min	SSA of 336.82 m^2 g^{-1}; Structural defects (I_D/I_G = 1.11) due to the co-doping of N and S and low graphitization	E_{onset}= 0.931 V; $E_{1/2}$= 0.82 V; j_L= −5.24 mA cm^{-2}; 4e− pathway (n=3.87); Tafel slope of 76 mV dec^{-1}	N,S-dual doping; Metal-N (Ta-N_x/Ta-OCN); Suboxide TaO_x species; Pyridinic and graphitic-N	Maliutina et al. (2021b)

In O_2-sat. 0.1 M KOH, otherwise specifically noted.

(Zhang et al., 2018) salts into a porous carbon catalyst can significantly improve the ORR catalytic performance of the resulting samples. Furthermore, nickel-based (Ding et al., 2019) carbon materials have been extensively considered as a highly efficient HER/OER electrocatalyst. In synthesis of bifunctional/trifunctional electrocatalysts, doping of metal or metal oxides onto a biomass-derived CNs may be an alternative manner. This section represents recent progress towards the next-generation of multifunctional hybrid metal-loaded green catalysts, as summarized in Table 2 and Supplementary Table S5. It can be seen in Table 2 and Supplementary Table S5, that the most of widespread metal-based interractions are presented by Fe-N_x (or Fe-N-C) and Co-N_x NPs (or Co-N-C) heterojunctions, i.e., a central TM cation coordinated to pyridinic nitrogen on edges of the graphitic surface. Despite that, pyridinic-N can be found as the most common active sive for ORR/OER of biomass-derived carbonaceous nanosupport.

Recently, Zhang et al. (2018) employed chitosan biomass for *in situ* synthesis of Co,N-codoped CNTs, amongst other N and Co doped nanosheets. It can be seen that the synthesized CNT electrocatalysts possess tubular morphology with uniform distribution of N and Co atoms. A sample of Co(16%) and N codoped CNT (Co16%-NCNT-T800) synthesized at 800°C has been found to display the highest ORR current density (6.92 mA cm^{-2}) among other carbon based catalysts and Pt (40 wt%)/C (5.06 mA cm^{-2}) and a half-wave potential closest to Pt (40 wt %)/C. In line with recent research showing that M–N–C active sites formed via coordination of the metal with pyridinic nitrogen plays a crucial role in enhancing ORR activities, Zhang et al. (2018) showed that key for high ORR activity is an effective formation of the Co–N–C active sites (via pyridinic nitrogen). The Authors also found that the Co16%-NCNT-T800 sample exhibited the highest specific capacitance of all electrocatalysts. The higher the specific capacitance (the latter resulting directly from electrochemical specific surface area), the higher the amount of active sites for current density enhancement. Furthemore, the as-prepared Co16%-NCNT-T800 electrocatalyst showed exceptional resistance to the

methanol poisoning with no obvious drop in current (in contrast to that of Pt/C benchmark) and long-time stability.

In a recent study, of Lv and others (Lv et al., 2019) fabricated a hierarchical porous Co,N-codoped bio-carbon bifunctional electrocatalyst (CoTBrPP@bio-C) for an all-pH ORR and HER by using a simple one-pot co-pyrolysis over a commercially available mushroom template with adsorbed Br-substituted porphyrinato cobalt (CoTBrPP). The as-prepared nanosheets displayed a porous stratified volcanic rock-like structure with Co-N_x functionalities. XPS was executed to determine the impact of Br on the formation and distribution of nitrogenized functionalities. Autors claimed that the addition of Br can promote the formation of Co-N_x and graphitic-N species, attributed to active centers for ORR and HER. Further, ORR and HER electrocatalytic activity were evaluated in 0.1 M KOH and 1 M KOH environments, respectively. The obtained biomass-derived CoTBrPP@bio-C hybrid electrocatalyst possessed outstanding activity towards ORR (E_{onset}=0.93 V vs. RHE and $E_{1/2}$=0.85 V vs. RHE) as well as HER activity. The excellent Zn-air battery performance of the CoTBrPP@bio-C hybrid with the open-circuit voltage remained at 1.51 V, while the discharging polarization and the corresponding power density of 100 mW cm^{-2} at 155 mA cm^{-2}, were superior to that of Pt/C (78 mW cm^{-2} at 119 mA cm^{-2}).

4 Nanostructured biochar: economic evaluation and circular economy approach

The physical-chemical characteristics of biochar, influenced by biomass type, thermal conversion, and preparation circumstances, contribute to its electrocatalytic activities. Altering these features through physical and chemical activation techniques can enhance biochar's surface functional groups, surface area, and porous structure. Biochar-based catalysts show potential as renewable alternatives to expensive benchmark noble-based materials. Using CNs from biochar offers economic and environmental benefits. However, addressing limitations and knowledge gaps is crucial, such as scaling up production and utilization of machine learning models.

In general, cost analysis of biochars production consist of the following crucial steps and factors: (a) feedstock purchase cost, (b) transportation costs, (c) synthetic/fabrication costs, (d) operating labor/employed personnel costs, (e) storage costs, (f) maintenance, insurance, and other costs. It was reported that a charcoal production stage (carbonization) cost 113 \$ ton^{-1} charcoal (Norgate and Langberg, 2009). Production stage cost for three different biochars production plants were studied (Shackley et al., 2011). Production stage cost including capital, storage, utility, labor and other plant cost ranged from 98 US\$ ton^{-1} to 353 US\$ ton^{-1} charcoal (Suopajärvi and Fabritius, 2013). A life cycle analysis for overall biochar production via the pyrolysis process found the great importance of biochar in the soil is the carbon sink effect which accounts for 50% of the total negative emissions (or contribution of −368 $kgCO_2$/ton of dried feedstock based on the carbon footprint calculation) (Costa et al., 2023). However, the lack of comprehensive studies on synergistic assessment of nanostructured biochar and the circular economy is remaining. Therefore, these areas need more attention and further investigation.

Furthermore, there is a gap in understanding the long-term performance and scalability of CNs derived from biomass. It is crucial to assess the durability and regeneration potential of nanostructured biochar, as well as its impact on the surrounding environment. Economic feasibility studies are also needed to evaluate the cost-effectiveness of implementing large-scale biochar treatment systems. Moreover, there is a need for comprehensive life cycle assessments to understand the overall environmental impacts of utilizing biomass-derived biochar in electrocatalytic systems. This includes assessing the carbon footprint, energy requirements, and potential by-products or emissions associated with its production and use. Addressing these innovation and research gaps will contribute to the development of efficient, sustainable, and economically viable biochar-based solutions for sustainable energy generation/storage within the circular economy framework.

Although, depending on the final target, biochars should be modified to improve certain functions. Thus, some of the future perspectives of nanostructured biochars to be used as cost-efficient electrocatalysts may include:

(0) Comparing the cost and overall electrochemical properties of biomass-derived NCs with other benchmark catalysts, such as Pt/C, doped CNTs, CNFs, graphene, *etc.*,;
(1) Study on the optimisation of price factor for maximum yield of nanomaterials at an optimum pyrolysis temperature/pressure/heating rate/reaction time/atmosphere *etc.*
(2) Conduct commercial scale cost analysis of nanostructured biochars production plant.
(3) *In situ* or post-treatment modification of biochar surfaces utilizing different modifying agents to achieve selectivity and optimum performance.

5 Conclusion and future horizons

In this review, we have discussed the recent advances in biomass-derived CNs as non-noble electrocatalysts with the sustainable goal of establishing an environmentally sensible circulation of energy and materials. The role of biomass originality and pretreatment methods were elucidated with a focus on the formation of CNs. The performance of recently reported biomass-derived CNs is discussed, reflecting on mechanistic understanding of principles for biomass conversion based on their origin. Specifically, the current status of the most superior biomass-derived electrocatalysts for the ORR/HER/OER based on a common set of figures of merit, namely, overpotential, half-wave potential, current density, stability, and durability, as well as methanol tolerance tests in case of ORR and OER were explored in detail. Various design strategies to construct a heteroatom-supported 2D or 3D nanocatalyst architecture promote a large number of active sites including doping/defect introduction, chemical functionalization/activation well as the synthesis method and conditions, were discussed. Furthermore, the need to elucidate the kinetics and reaction barriers at the electrolyte-electrode interface and the modalities of electron/proton transfers cannot be exaggerated. In this regard, one of the main conclusions is to establish an integrated scheme to

strengthen both experimental and theoretical insightful tools towards the design, synthesis, characterization, and testing of feasibility for practical catalyst systems. Despite significant progress made as discussed above, there are still many challenges ahead in the development of electrocatalysts for ORR/HER/OER, and further efforts are also required to elucidate other factors that can expedite the advancements. Prospective research studies in this regard can focus on the following:

(1) An in-depth understanding of the related mechanism for each reaction, especially over specific facile biomass-derived nanostructures, will provide a knowledge-driven scheme for the design and development of efficient catalysts by optimizing computational studies towards reaction mechanisms. Specifically, the investigation into the mechanism can guide structural modification, electronic reconfiguration, and prevention of catalyst active site degradation during cycling. Most reported computational studies are based on simplified synthetic precursor-derived models and lack accurate prediction of the actual kinetics and reaction mechanisms at given operating conditions.

(2) Morphology-engineered metal-free biomass-derived nanostructures have demonstrated high-performance efficacy and stability in the considered electrocatalytic processes. On this account, the catalyst with abundant active sites can be fabricated into specific configurations (such as nanosheets, CNTs/CNFs) to improve the catalysts' physiochemical properties. By so doing, the porosity and number of accessible active sites are increased; hence, facilitating species adsorption, activation, and electron diffusion. Therefore, the construct of these nanocatalysts must be optimized.

(3) Generally, the extensive integration of computational and experimental studies in the construct of catalyst systems is lacking, particularly in the fabrication methods for the engineered catalysts. Most reported studies in this regard are theory-based, with little or no detailing of experimental schemes to effectuate the newly developed catalyst active sites. Ideally, integrating all mechanistic information demands a rigorous standardization of experimental setups and procedures, in-depth understanding beyond surficial catalyst interactions, and multi-scale modeling entailing all these aspects.

(4) Thorough knowledge based on the above outlooks is essential to developing novel or improved electrocatalysts. Thereupon, the controlled development of functional nanostructured composites with better catalytic activity and stability from biomass is not far-fetched. For instance, various heteroatom-doped functional carbon-based nanomaterials or metal-added hybrids have displayed exceptional potential towards overall water splitting due to their tuneable structure, available active sites, and durability in alkaline/acidic electrolytes. In summary, the optimization of these advanced functional materials is vital to the practical application of these processes.

(5) In addition to the optimization of composite catalysts, measures can be adopted to expedite this process via accelerating catalyst discovery. Due to advancements in machine learning and material genome databases, accelerating catalyst discovery by high-throughput assessment and non-supervised analytical techniques such as AI algorithms, aided with identifying key synthetic parameters, is realistic. *In situ* and *an operando* studies are highly required for online evaluation of reaction kinetics, such as *in situ* Raman spectroscopy, *in situ* electron paramagnetic resonance (EPR) *in situ* differential electrochemical mass spectrometry (DEMS). Moreover, the state-of-the-art computer-aided robotic and automated facilities enable autonomous and controlled nanocatalyst synthesis from biomass precursors, characterization, and performance evaluation, which could significantly boost discovery of the advanced catalysts for electrochemical conversion of water and other molecules such as ammonia and carbon dioxide.

(7) According to recent life-cycle assessment (LCA) studies, nanostructured biochars are promising and economic feasible materials that are believed to provide multiple-advantages for both environmental and agricultural activities and the future practical implementation of electrochemical systems. Moreover, no literature has mentioned the deployment of circular economy in the combination of biomass/waste derived CNs and electrochemical systems/devices toward the benefits of alternative energy generation and storage. Therefore, to facilitate the progression of the carbon-negative circular economy, the future directions of applying biomass/waste-derived CNs can be suggested, i.e., (1) establishing regional circular centres utilizing various biomasses and wastes, (2) advancing the electrochemical systems and storage devices towards large-scale demonstration, and (3) evaluating the environmental benefits, potential harms, and CO2 reduction potentials.

(8) Based on observed literature scope we summarise the following factors towards efficient generation of CNs from biomass for electrochemical approaches: (a) the optimal temperature range for maximized yield of CNs in biochar is between 450°C and 800 °C. Different feedstocks require specific pyrolyzing temperatures due to their particular structures and chemical compositions: lignocellulosic-based generally require higher temperatures for decomposition/biochar formation compare to that non-lignocellulosic biomass; (b) generally, the maximized CNs yield in biochar was reported for pyrolysis in oxygen-limited or nitrogen atmosphere for reaction time between 1 and 2 h; (c) microwave-assisted pyrolysis can significantly decrease the pyrolysis time and facilitate the formation and grow of CNTs/CNFs features due to proposed CVD mechanisms.

(9) For large-scale and cost-effective implementation in the cutting-edge fuel cells, water splitting systems, supercapacitors, and rechargeable batteries, it is necessary to maintain the efficiency of biomass conversion and the quality of CNs without additional processing step. During the functionalization of biochar (i.e., surface oxidation, amination, sulfonation, *etc.*), complex operations and toxic chemicals should be avoided in order to preserve an environmentally friendly solution. Regardless of the pre/post-treatments, residual impurities can always remain in the biochar, which can negatively affect the operation of the

devices. Develop strategies to reduce the content of impurities to an acceptable minimum is necessary.

(10) In view of the technological advancement in this field, researchers underscore the importance of developing more resolute legal and techno-economic frameworks that can successfully promote sustainable solutions by internalizing environmental costs and hinder drawbacks. Overall, a level of parallelism between the technological, economic and legal aspects of these technologies both at the initial stage of development and coordinated efforts based on a long-term view should be established. However, the processes are still a long way away from global practical application and feasibility tests on a pilot scale for the highly efficient biomass-derived nanomaterials are paramount on the way for a sustainable future.

Author contributions

KM: Investigation, Validation, Data curation, Formal analysis, Visualization, Writing—original draft, Writing—review and editing. JO: Software, Data curation, Writing—review and editing. CH: Software, Formal analysis, Writing—review and editing. LF: Formal analysis, Writing—review and editing, Supervision, Project administration, Funding acquisition. AF: Conceptualization, Methodology, Resources, Writing—review and editing, Project administration, Funding acquisition.

Funding

This work was supported by the Natural Science Foundation of Guangdong Province (2021A1515012356), the Scientific Foundation of Guangdong Provincial Education Department (2019KTSCX151), Shenzhen Government's Plan of Science and Technology (JCYJ20180305125247308), and the National Natural Science Foundation of China (51402093). The Net Zero Innovation Institute of Cardiff University is kindly acknowledged for supporting AF via a University Research Fellowship in Electrocatalysis.

Conflict of interest

The authors declare that the research was conducted in the absence of any commercial or financial relationships that could be construed as a potential conflict of interest.

The author(s) AF declared that they were an editorial board member of Frontiers, at the time of submission. This had no impact on the peer review process and the final decision.

Publisher's note

Supplementary material

The Supplementary Material for this article can be found online at: https://www.frontiersin.org/articles/10.3389/fenve.2023.1228992/full#supplementary-material

References

Abdelkareem, M. A., Elsaid, K., Wilberforce, T., Kamil, M., Sayed, E. T., and Olabi, A. (2021). Environmental aspects of fuel cells: a review. *Sci. Total Environ.* 752, 141803. doi:10.1016/j.scitotenv.2020.141803

Abraham, E., Deepa, B., Pothan, L., Jacob, M., Thomas, S., Cvelbar, U., et al. (2011). Extraction of nanocellulose fibrils from lignocellulosic fibres: a novel approach. *Carbohydr. Polym.* 86, 1468–1475. doi:10.1016/j.carbpol.2011.06.034

Akula, S., Varathan, P., Menon, R. S., and Sahu, A. K. (2021). Rationally constructing nitrogen–fluorine heteroatoms on porous carbon derived from pomegranate fruit peel waste towards an efficient oxygen reduction catalyst for polymer electrolyte membrane fuel cells. *Sustain. Energy & Fuels* 5, 886–899. doi:10.1039/d0se01214a

Alston, S. M., and Arnold, J. C. (2011). Environmental impact of pyrolysis of mixed WEEE plastics Part 2: life cycle assessment. *Environ. Sci. Technol.* 45, 9386–9392. doi:10.1021/es2016654

Amiinu, I. S., Zhang, J., Kou, Z., Liu, X., Asare, O. K., Zhou, H., et al. (2016). Self-organized 3D porous graphene dual-doped with biomass-sponsored nitrogen and sulfur for oxygen reduction and evolution. *ACS Appl. Mat. Interfaces* 8, 29408–29418. doi:10.1021/acsami.6b08719

Anca-Couce, A. (2016). Reaction mechanisms and multi-scale modelling of lignocellulosic biomass pyrolysis. *Prog. Energy Combust. Sci.* 53, 41–79. doi:10.1016/j.pecs.2015.10.002

Andrews, R., Jacques, D., Qian, D., and Dickey, E. C. (2001). Purification and structural annealing of multiwalled carbon nanotubes at graphitization temperatures. *Carbon* 39, 1681–1687. doi:10.1016/s0008-6223(00)00301-8

Bhaskar, T., Bhavya, B., Singh, R., Naik, D. V., Kumar, A., and Goyal, H. B. (2011). "Chapter 3 - thermochemical conversion of biomass to biofuels," in *Biofuels*. Editors A. Pandey, C. Larroche, S. C. Ricke, C.-G. Dussap, and E. Gnansounou (Amsterdam: Academic Press), 51–77.

Bikbulatova, S., Tahmasebi, A., Zhang, Z., and Yu, J. (2017). Characterization and behavior of water in lignocellulosic and microalgal biomass for thermochemical conversion, Fuel Process. *Fuel Process. Technol.* 160, 121–129. doi:10.1016/j.fuproc.2017.02.025

Borghei, M., Laocharoen, N., Kibena-Põldsepp, E., Johansson, L.-S., Campbell, J., Kauppinen, E., et al. (2017). Porous N,P-doped carbon from coconut shells with high electrocatalytic activity for oxygen reduction: alternative to Pt-C for alkaline fuel cells. *Appl. Catal. B Environ.* 204, 394–402. doi:10.1016/j.apcatb.2016.11.029

Cai, C. L., Liu, Q. Y., and Wang, T. J. (2015). Progress on reaction pathway and catalysts for preparation of long chain alkanes from lignocellulosic biomass. *Chem. Ind. For. Prod.* 35, 153–162. doi:10.3969/j.issn.0253-2417.2015.06.025

Chang, Y., Shi, H., Yan, X., Zhang, G., and Chen, L. (2020). A ternary B, N, P-Doped carbon material with suppressed water splitting activity for high-energy aqueous supercapacitors. *Carbon* 170, 127–136. doi:10.1016/j.carbon.2020.08.013

Chaparro-Garnica, J., Salinas-Torres, D., Mostazo-López, M. J., Morallón, E., and Cazorla-Amorós, D. (2021). Biomass waste conversion into low-cost carbon-based materials for supercapacitors: a sustainable approach for the energy scenario. *J. Electroanal. Chem.* 880, 114899. doi:10.1016/j.jelechem.2020.114899

Chen, C., Yu, D., Zhao, G., Du, B., Tang, W., Sun, L., et al. (2016). Three-dimensional scaffolding framework of porous carbon nanosheets derived from plant wastes for high-performance supercapacitors. *Nano Energy* 27, 377–389. doi:10.1016/j.nanoen.2016.07.020

Chen, H. (2014). *Chemical composition and structure of natural lignocellulose, biotechnol, lignocell.* Dordrecht: Springer, 25–71.

Chen, P., Wang, L.-K., Wang, G., Gao, M.-R., Ge, J., Yuan, W.-J., et al. (2014). Nitrogen-doped nanoporous carbon nanosheets derived from plant biomass: an efficient catalyst for oxygen reduction reaction. *Energy Environ. Sci.* 7, 4095–4103. doi:10.1039/c4ee02531h

Chen, Y., and Chadderton, L. T. (2004). Improved growth of aligned carbon nanotubes by mechanical activation. *J. Mater. Res.* 19, 2791–2794. doi:10.1557/jmr.2004.0398

Chen, Y., and Yu, J. (2005). Growth direction control of aligned carbon nanotubes. *Carbon* 43, 3183–3186. doi:10.1016/j.carbon.2005.07.015

Cheng, C., Li, Y., Maouche, C., Li, B., Zhou, Y., Wang, S., et al. (2021). Green synthesis of N, P-co doped porous reduced graphene oxide as an active metal-free electrocatalyst toward oxygen reduction reaction. *J. Electroanal. Chem.* 883, 115058. doi:10.1016/j.jelechem.2021.115058

Costa, J. A. V., Zaparoli, M., Cassuriaga, A. P. A., Cardias, B. B., Vaz, B. d. S., Morais, M. G. d., et al. (2023). Biochar production from microalgae: a new sustainable approach to wastewater treatment based on a circular economy. *Enzyme Microb. Technol.* 169, 110281. doi:10.1016/j.enzmictec.2023.110281

Dekel, D. R. (2018). Review of cell performance in anion exchange membrane fuel cells. *J. Power Sources* 375, 158–169. doi:10.1016/j.jpowsour.2017.07.117

Ding, J., Ji, S., Wang, H., Gai, H., Liu, F., Linkov, V., et al. (2019). Mesoporous nickel-sulfide/nickel/N-doped carbon as HER and OER bifunctional electrocatalyst for water electrolysis. *Int. J. Hydrogen Energy* 44, 2832–2840. doi:10.1016/j.ijhydene.2018.12.031

Fan, L., Zhu, B., Su, P.-C., and He, C. (2018). Nanomaterials and technologies for low temperature solid oxide fuel cells: recent advances, challenges and opportunities. *Nano Energy* 45, 148–176. doi:10.1016/j.nanoen.2017.12.044

Feng, H., Xu, Z., Ren, L., Liu, C., Zhuang, J., Hu, Z., et al. (2018). Activating titania for efficient electrocatalysis by vacancy engineering. *ACS Catal.* 8, 4288–4293. doi:10.1021/acscatal.8b00719

Gao, S., Sun, Z., Liu, W., Jiao, X., Zu, X., Hu, Q., et al. (2017). Atomic layer confined vacancies for atomic-level insights into carbon dioxide electroreduction. *Nat. Commun.* 8, 14503. doi:10.1038/ncomms14503

Gong, K., Du, F., Xia, Z., Durstock, M., and Dai, L. J. s. (2009). Nitrogen-doped carbon nanotube arrays with high electrocatalytic activity for oxygen reduction. *Science* 323, 760–764. doi:10.1126/science.1168049

Gong, Y., Yang, Z., Lin, Y., Zhou, T., Li, J., Jiao, F., et al. (2019). Correction: controlled synthesis of bifunctional particle-like Mo/Mn-NixSy/NF electrocatalyst for highly efficient overall water splitting. *Dalton Trans.* 48, 7025. doi:10.1039/c9dt90089f

Goodell, B., Xie, X., Qian, Y., Daniel, G., Peterson, M., and Jellison, J. (2008). Carbon nanotubes produced from natural cellulosic materials. *J. Nanosci. Nanotechnol.* 8, 2472–2474. doi:10.1166/jnn.2008.235

Guo, D., Shibuya, R., Akiba, C., Saji, S., Kondo, T., and Nakamura, J. (2016). Active sites of nitrogen-doped carbon materials for oxygen reduction reaction clarified using model catalysts. *Science* 351, 361–365. doi:10.1126/science.aad0832

Han, L., Cui, X., Liu, Y., Han, G., Wu, X., Xu, C., et al. (2020). Nitrogen and phosphorus modification to enhance the catalytic activity of biomass-derived carbon toward the oxygen reduction reaction. *Sustain. Energy & Fuels* 4, 2707–2717. doi:10.1039/c9se00985j

Han, M., Shi, M., Wang, J., Zhang, M., Yan, C., Jiang, J., et al. (2019). Efficient bifunctional Co/N dual-doped carbon electrocatalysts for oxygen reduction and evolution reaction. *Carbon* 153, 575–584. doi:10.1016/j.carbon.2019.07.075

Harmsen, P. F. H., Huijgen, W., Bermudez, L., and Bakker, R. (2010). *Literature review of physical and chemical pretreatment processes for lignocellulosic biomass*. Wageningen, Netherlands: Food Biobased Research, 1–49.

He, D., Zhao, W., Li, P., Liu, Z., Wu, H., Liu, L., et al. (2019). Bifunctional biomass-derived 3D nitrogen-doped porous carbon for oxygen reduction reaction and solid-state supercapacitor. *Appl. Surf. Sci.* 465, 303–312. doi:10.1016/j.apsusc.2018.09.185

Hori, Y., Kikuchi, K., Murata, A., and Suzuki, S. (1986). Production of methane and ethylene in electrochemical reduction of carbon dioxide at copper electrode in aqueous hydrogencarbonate solution. *Chem. Lett.* 15, 897–898. doi:10.1246/cl.1986.897

Hori, Y., Kikuchi, K., and Suzuki, S. (1985). Production of CO and CH_4 in electrochemical reduction of CO_2 at metal electrodes in aqueous hydrogencarbonate solution. *Chem. Lett.* 14, 1695–1698. doi:10.1246/cl.1985.1695

Hori, Y., Murata, A., and Takahashi, R. (1989). Formation of hydrocarbons in the electrochemical reduction of carbon dioxide at a copper electrode in aqueous solution. *J. Chem. Soc.* 85, 2309–2326. doi:10.1039/f19898502309

Huang, B., Liu, Y., Huang, X., and Xie, Z. (2018). Multiple heteroatom-doped few-layer carbons for the electrochemical oxygen reduction reaction. *J. Mat. Chem. A* 6, 22277–22286. doi:10.1039/c8ta06743k

Huang, B., Liu, Y., Wei, Q., and Xie, Z. (2019). Three-dimensional mesoporous graphene-like carbons derived from a biomolecule exhibiting high-performance oxygen reduction activity. *Sustain. Energy & Fuels* 3, 2809–2818. doi:10.1039/c9se00365g

Huang, B., Liu, Y., and Xie, Z. (2017). Biomass derived 2D carbons via a hydrothermal carbonization method as efficient bifunctional ORR/HER electrocatalysts. *J. Mat. Chem. A* 5, 23481–23488. doi:10.1039/c7ta08052b

Huang, J., Su, T., Zhao, H., Li, F., Chiu, T.-W., Singh, M., et al. (2022). Nano and phase engineering of Fe-Cu alloy exsolved perovskite oxide-based hetero-catalysts for efficient oxygen evolution reaction. *Fuel* 356, 129479. doi:10.1016/j.fuel.2023.129479

Huang, N.-b., Zhang, J.-j., Sun, Y., Sun, X.-n., Qiu, Z.-y., and Ge, X.-w. (2020). A non-traditional biomass-derived N, P, and S ternary self-doped 3D multichannel carbon ORR electrocatalyst. *New J. Chem.* 44, 14604–14614. doi:10.1039/d0nj03283b

Huang, Y.-F., Chiueh, P.-T., and Lo, S.-L. (2016). A review on microwave pyrolysis of lignocellulosic biomass. *Sustain. Environ. Res.* 26, 103–109. doi:10.1016/j.serj.2016.04.012

Hwang, J., Rao, R. R., Giordano, L., Katayama, Y., Yu, Y., and Shao-Horn, Y. (2017). Perovskites in catalysis and electrocatalysis. *Science* 358, 751–756. doi:10.1126/science.aam7092

Inagaki, M., Toyoda, M., Soneda, Y., and Morishita, T. (2018). Nitrogen-doped carbon materials. *Carbon* 132, 104–140. doi:10.1016/j.carbon.2018.02.024

Ito, Y., Cong, W., Fujita, T., Tang, Z., and Chen, M. J. A. C. (2015). High catalytic activity of nitrogen and sulfur co-doped nanoporous graphene in the hydrogen evolution reaction. *Angew. Chem.* 127, 2159–2164. doi:10.1002/ange.201410050

Jatav, H., Goyam, S., Kumar, V., Jayant, H., Chattopadhyay, A., Dhawal, S., et al. (2017). Role of biochar: in agriculture sector its implication and perspective. *Int. J. Chem. Stud.* 14, 14–18.

Jiang, H., Gu, J. X., Zheng, X. S., Liu, M., Qiu, X. Q., Wang, L. B., et al. (2019a). Defect-rich and ultrathin N doped carbon nanosheets as advanced trifunctional metal-free electrocatalysts for the ORR, OER and HER. *Energy Environ. Sci.* 12, 322–333. doi:10.1039/c8ee03276a

Jiang, H., Gu, J., Zheng, X., Liu, M., Qiu, X., Wang, L., et al. (2019b). Defect-rich and ultrathin N doped carbon nanosheets as advanced trifunctional metal-free electrocatalysts for the ORR, OER and HER. *Energy Environ. Sci.* 12, 322–333. doi:10.1039/c8ee03276a

Jordan, J., and Smith, P. T. (1960). Free-radical intermediate in the electroreduction of carbon dioxide. *Proceed. Chem. Soc.* 1960, 246–247.

Kabir, G., and Hameed, B. H. (2017). Recent progress on catalytic pyrolysis of lignocellulosic biomass to high-grade bio-oil and bio-chemicals. *Renew. Sustain. Energy Rev.* 70, 945–967. doi:10.1016/j.rser.2016.12.001

Kang, Z., Wang, E., Mao, B., Su, Z., Chen, L., and Xu, L. (2005). Obtaining carbon nanotubes from grass. *Nanotechnology* 16, 1192–1195. doi:10.1088/0957-4484/16/8/036

Keiluweit, M., Nico, P. S., Johnson, M. G., and Kleber, M. (2010). Dynamic molecular structure of plant biomass-derived black carbon (biochar). *Environ. Sci. Technol.* 44, 1247–1253. doi:10.1021/es9031419

Khiari, B., Jeguirim, M., Limousy, L., and Bennici, S. (2019). Biomass derived chars for energy applications. *Renew. Sustain. Energy Rev.* 108, 253–273. doi:10.1016/j.rser.2019.03.057

Kosinkova, J., Doshi, A., Maire, J., Ristovski, Z., Brown, R., and Rainey, T. J. (2015). Measuring the regional availability of biomass for biofuels and the potential for microalgae. *Renew. Sustain. Energy Rev.* 49, 1271–1285. doi:10.1016/j.rser.2015.04.084

Kreuter, W., and Hofmann, H. (1998). Electrolysis: the important energy transformer in a world of sustainable energy. *Int. J. Hydrogen Energy* 23, 661–666. doi:10.1016/s0360-3199(97)00109-2

Kumar, R., Singh, R. K., and Singh, D. (2016). Natural and waste hydrocarbon precursors for the synthesis of carbon based nanomaterials: graphene and CNTs. *Renew. Sustain. Energy Rev.* 58, 976–1006. doi:10.1016/j.rser.2015.12.120

Kuznetsov, V. L., Usoltseva, A. N., Chuvilin, A. L., Obraztsova, E. D., and Bonard, J.-M. (2001). Thermodynamic analysis of nucleation of carbon deposits on metal particles and its implications for the growth of carbon nanotubes. *Phys. Rev. B* 64, 235401. doi:10.1103/physrevb.64.235401

Lai, L., Potts, J. R., Zhan, D., Wang, L., Poh, C. K., Tang, C., et al. (2012). Exploration of the active center structure of nitrogen-doped graphene-based catalysts for oxygen reduction reaction. *Energy Environ. Sci.* 5, 7936–7942. doi:10.1039/c2ee21802j

Lee, J., Kim, K.-H., and Kwon, E. E. (2017). Biochar as a catalyst. *Renew. Sustain. Energy Rev.* 77, 70–79. doi:10.1016/j.rser.2017.04.002

Lei, Y., Yang, F., Xie, H., Lei, Y., Liu, X., Si, Y., et al. (2020). Biomass *in situ* conversion to Fe single atomic sites coupled with Fe2O3 clusters embedded in porous carbons for the oxygen reduction reaction. *J. Mat. Chem. A* 8, 20629–20636. doi:10.1039/d0ta06022d

Li, D. C., and Jiang, H. (2017). The thermochemical conversion of non-lignocellulosic biomass to form biochar: a review on characterizations and mechanism elucidation. *Bioresour. Technol.* 246, 57–68. doi:10.1016/j.biortech.2017.07.029

Li, F., Mushtaq, N., Su, T., Cui, Y., Huang, J., Sun, M., et al. (2023). NCNT grafted perovskite oxide as an active bifunctional electrocatalyst for rechargeable zinc-air battery. *Mater. Today Nano* 21, 100287. doi:10.1016/j.mtnano.2022.100287

Li, F., Yin, Y., Zhang, C., Li, W., Maliutina, K., Zhang, Q., et al. (2020a). Enhancing oxygen reduction performance of oxide-CNT through *in-situ* generated nanoalloy bridging. *Appl. Catal. B Environ.* 263, 118297. doi:10.1016/j.apcatb.2019.118297

Li, J.-C., Qin, X., Hou, P.-X., Cheng, M., Shi, C., Liu, C., et al. (2019c). Identification of active sites in nitrogen and sulfur co-doped carbon-based oxygen reduction catalysts. *Carbon* 147, 303–311. doi:10.1016/j.carbon.2019.01.018

Li, W., Yin, Y., Xu, K., Li, F., Maliutina, K., Wu, Q., et al. (2021). Enhancement of oxygen evolution activity of perovskite $(La_{0.8}Sr_{0.2})_{0.95}MnO_{3-\delta}$ electrode by Co phase surface modification. *Catal. Today* 364, 148–156. doi:10.1016/j.cattod.2020.02.015

Li, X., Zhang, Y., Zhang, J., and Wang, C. (2019d). Isolated Fe atoms dispersed on cellulose-derived nanocarbons as an efficient electrocatalyst for the oxygen reduction reaction. *Nanoscale* 11, 23110–23115. doi:10.1039/c9nr07914a

Li, Y. (2014). *Studies on cellulose hydrolysis and hemicellulose monosaccharide degradation in concentrated hydrochloric acid*. Ottawa: University of Ottawa. Master of Applied Science.

Li, Y., Wang, G., Wei, T., Fan, Z., and Yan, P. (2016). Nitrogen and sulfur co-doped porous carbon nanosheets derived from willow catkin for supercapacitors. *Nano Energy* 19, 165–175. doi:10.1016/j.nanoen.2015.10.038

Li, Y., Wen, H., Yang, J., Zhou, Y., and Cheng, X. (2019a). Boosting oxygen reduction catalysis with N, F, and S tri-doped porous graphene: tertiary N-precursors regulates the constitution of catalytic active sites. *Carbon* 142, 1–12. doi:10.1016/j.carbon.2018.09.079

Li, Y., Xing, B., Ding, Y., Han, X., and Wang, S. (2020b). A critical review of the production and advanced utilization of biochar via selective pyrolysis of lignocellulosic biomass. *Bioresour. Technol.* 312, 123614. doi:10.1016/j.biortech.2020.123614

Li, Y., Zhou, L. W., and Wang, R. Z. (2017). Urban biomass and methods of estimating municipal biomass resources. *Renew. Sustain. Energy Rev.* 80, 1017–1030. doi:10.1016/j.rser.2017.05.214

Li, Z., Wang, L., Li, Y., Feng, Y., and Feng, W. (2019b). Carbon-based functional nanomaterials: preparation, properties and applications. *Compos. Sci. Technol.* 179, 10–40. doi:10.1016/j.compscitech.2019.04.028

Lin, Y.-C., and Huber, G. W. (2009). The critical role of heterogeneous catalysis in lignocellulosic biomass conversion. *Energy Environ. Sci.* 2, 68–80. doi:10.1039/b814955k

Liu, R., Wang, Y., Liu, D., Zou, Y., and Wang, S. (2017). Water-plasma-enabled exfoliation of ultrathin layered double hydroxide nanosheets with multivacancies for water oxidation. *Adv. Mater.* 29, 1701546. doi:10.1002/adma.201701546

Liu, W.-J., Jiang, H., and Yu, H.-Q. (2015a). Development of biochar-based functional materials: toward a sustainable platform carbon material. *Mater.* ***Chem. Rev.*** 115, 12251–12285. doi:10.1021/acs.chemrev.5b00195

Liu, W.-J., Jiang, H., and Yu, H.-Q. (2019). Emerging applications of biochar-based materials for energy storage and conversion. *Energy Environ. Sci.* 12, 1751–1779. doi:10.1039/c9ee00206e

Liu, W.-J., Jiang, H., and Yu, H.-Q. (2015b). Thermochemical conversion of lignin to functional materials: a review and future directions. *Green Chem.* 17, 4888–4907. doi:10.1039/c5gc01054c

Liu, Z., Wang, F., Li, M., and Ni, Z.-H. (2016). N, S and P-ternary doped carbon nanopore/tube composites derived from natural chemicals in waste sweet osmanthus fruit with superior activity for oxygen reduction in acidic and alkaline media. *RSC Adv.* 6, 37500–37505. doi:10.1039/c6ra08371d

Lu, Z., Wang, J., Huang, S., Hou, Y., Li, Y., Zhao, Y., et al. (2017). N,B-codoped defect-rich graphitic carbon nanocages as high performance multifunctional electrocatalysts. *Nano Energy* 42, 334–340. doi:10.1016/j.nanoen.2017.11.004

Lv, X., Chen, Y., Wu, Y., Wang, H., Wang, X., Wei, C., et al. (2019). A Br-regulated transition metal active-site anchoring and exposure strategy in biomass-derived carbon nanosheets for obtaining robust ORR/HER electrocatalysts at all pH values. *J. Mat. Chem. A* 7, 27089–27098. doi:10.1039/c9ta10880g

Mahmoudian, L., Rashidi, A., Dehghani, H., and Rahighi, R. (2016). Single-step scalable synthesis of three-dimensional highly porous graphene with favorable methane adsorption. *Chem. Eng. J.* 304, 784–792. doi:10.1016/j.cej.2016.07.015

Maliutina, K., He, C. J., Huang, J. J., Yu, J. L., Li, F. J., He, C. X., et al. (2021b). Structural and electronic engineering of biomass-derived carbon nanosheet composite for electrochemical oxygen reduction. *Sustain. Energy & Fuels* 5, 2114–2126. doi:10.1039/d0se01631d

Maliutina, K., Huang, J., Su, T., Yu, J., and Fan, L. (2021a). Biomass-derived Ta,N,S co-doped CNTs enriched carbon catalyst for efficient electrochemical oxygen reduction. *J. Alloys Compd.* 888, 161479. doi:10.1016/j.jallcom.2021.161479

Maliutina, K., Tahmasebi, A., Yu, J., and Saltykov, S. N. (2017). Comparative study on flash pyrolysis characteristics of microalgal and lignocellulosic biomass in entrained-flow reactor. *Energy Convers. Manag.* 151, 426–438. doi:10.1016/j.enconman.2017.09.013

Maliutina, K., Tahmasebi, A., and Yu, J. (2018). The transformation of nitrogen during pressurized entrained-flow pyrolysis of Chlorella vulgaris. *Bioresour. Technol.* 262, 90–97. doi:10.1016/j.biortech.2018.04.073

Mamtani, K., Jain, D., Dogu, D., Gustin, V., Gunduz, S., Co, A. C., et al. (2018). Insights into oxygen reduction reaction (ORR) and oxygen evolution reaction (OER) active sites for nitrogen-doped carbon nanostructures (CNx) in acidic media. *Appl. Catal. B Environ.* 220, 88–97. doi:10.1016/j.apcatb.2017.07.086

Martín, A. J., and Pérez-Ramírez, J. (2019). Heading to distributed electrocatalytic conversion of small abundant molecules into fuels, chemicals, and fertilizers. *Joule* 3, 2602–2621. doi:10.1016/j.joule.2019.09.007

Martin, M. A. (2010). First generation biofuels compete. *New Biotechnol.* 27, 596–608. doi:10.1016/j.nbt.2010.06.010

Maruyama, S., Kojima, R., Miyauchi, Y., Chiashi, S., and Kohno, M. (2002). Low-temperature synthesis of high-purity single-walled carbon nanotubes from alcohol. *Chem. Phys. Lett.* 360, 229–234. doi:10.1016/s0009-2614(02)00838-2

Matter, P. H., Zhang, L., and Ozkan, U. S. (2006). The role of nanostructure in nitrogen-containing carbon catalysts for the oxygen reduction reaction. *J. Catal.* 239, 83–96. doi:10.1016/j.jcat.2006.01.022

Meshitsuka, S., Ichikawa, M., and Tamaru, K. (1974). Electrocatalysis by metal phthalocyanines in the reduction of carbon dioxide. *J. Chem. Soc. Chem. Commun.* 1974, 158–159. doi:10.1039/c39740000158

Mulyadi, A., Zhang, Z., Dutzer, M., Liu, W., and Deng, Y. (2017). Facile approach for synthesis of doped carbon electrocatalyst from cellulose nanofibrils toward high-performance metal-free oxygen reduction and hydrogen evolution. *Nano Energy* 32, 336–346. doi:10.1016/j.nanoen.2016.12.057

Munawar, M. A., Khoja, A. H., Naqvi, S. R., Mehran, M. T., Hassan, M., Liaquat, R., et al. (2021). Challenges and opportunities in biomass ash management and its utilization in novel applications. *Renew. Sustain. Energy Rev.* 150, 111451. doi:10.1016/j.rser.2021.111451

Nie, Y., Li, L., and Wei, Z. (2015). Recent advancements in Pt and Pt-free catalysts for oxygen reduction reaction. *Chem. Soc. Rev.* 44, 2168–2201. doi:10.1039/c4cs00484a

Niu, H.-J., Wang, A.-J., Zhang, L., and Feng, J.-J. (2020). Bioinspired one-step pyrolysis fabrication of 3D porous Co, N, P-doped carbon nanosheets with enriched $CoN_{<i>x</i>}$ active sites as high-performance bifunctional oxygen electrocatalyst for rechargeable Zn–air battery. *ACS Appl. Energy Mat.* 3, 2781–2790. doi:10.1021/acsaem.9b02450

Norgate, T., and Langberg, D. (2009). Environmental and economic aspects of charcoal use in steelmaking. *ISIJ Int.* 49, 587–595. doi:10.2355/isijinternational.49.587

Omoriyekomwan, J. E., Tahmasebi, A., Dou, J., Tian, L., and Yu, J. (2021a). Mechanistic study on the formation of silicon carbide nanowhiskers from biomass cellulose char under microwave. *Mater. Chem. Phys.* 262, 124288. doi:10.1016/j.matchemphys.2021.124288

Omoriyekomwan, J. E., Tahmasebi, A., Dou, J., Wang, R., and Yu, J. (2021b). A review on the recent advances in the production of carbon nanotubes and carbon nanofibers via microwave-assisted pyrolysis of biomass. *Fuel Process. Technol.* 214, 106686. doi:10.1016/j.fuproc.2020.106686

Omoriyekomwan, J. E., Tahmasebi, A., and Yu, J. (2016). Production of phenol-rich bio-oil during catalytic fixed-bed and microwave pyrolysis of palm kernel shell. *Bioresour. Technol.* 207, 188–196. doi:10.1016/j.biortech.2016.02.002

Omoriyekomwan, J. E., Tahmasebi, A., Zhang, J., and Yu, J. (2017). Formation of hollow carbon nanofibers on bio-char during microwave pyrolysis of palm kernel shell. *Energy Convers. Manag.* 148, 583–592. doi:10.1016/j.enconman.2017.06.022

Omoriyekomwan, J. E., Tahmasebi, A., Zhang, J., and Yu, J. L. (2019). Mechanistic study on direct synthesis of carbon nanotubes from cellulose by means of microwave pyrolysis. *Energy Convers. Manag.* 192, 88–99. doi:10.1016/j.enconman.2019.04.042

Onishchenko, D. V., Reva, V. P., Chakov, V. V., Kuryavyi, V. G., and Petrov, V. V. (2013a). Promising nanocomposite materials based on renewable plant resources. *Metallurgist* 56, 679–683. doi:10.1007/s11015-013-9635-y

Onishchenko, D. V., Reva, V. P., and Kuryavyi, V. G. (2012). Vacuum annealing of carbon nanotubes produced from amorphous carbon. *Coke Chem.* 55, 467–469. doi:10.3103/s1068364x12120034

Onishchenko, D. V., Reva, V. P., and Voronov, B. A. (2013b). Farm crop waste as a promising resource for forming carbon nanotubes. *Russ. Agric. Sci.* 39, 540–543. doi:10.3103/s1068367413050121

Prakash Menon, M., Selvakumar, R., Suresh kumar, P., and Ramakrishna, S. (2017). Extraction and modification of cellulose nanofibers derived from biomass for environmental application. *RSC Adv.* 7, 42750–42773. doi:10.1039/c7ra06713e

Ramanayaka, S., Vithanage, M., Alessi, D. S., Liu, W.-J., Jayasundera, A. C. A., and Ok, Y. S. (2020). Nanobiochar: production, properties, and multifunctional applications. *Environ. Sci. Nano* 7, 3279–3302. doi:10.1039/d0en00486c

Rao, C. V., Cabrera, C. R., and Ishikawa, Y. (2010). In search of the active site in nitrogen-doped carbon nanotube electrodes for the oxygen reduction reaction. *J. Phys. Chem. Lett.* 1, 2622–2627. doi:10.1021/jz100971v

Reva, V. P., Filatenkov, A. É., Mansurov, Y. N., and Kuryavyi, V. G. (2016a). Stages in multilayer carbon nanotube formation with mechanical activation of amorphous carbon. *Refract. Industrial Ceram.* 57, 141–145. doi:10.1007/s11148-016-9943-4

Reva, V. P., Filatenkov, A. E., Yagofarov, V. U., Gulevskii, D. A., Kuryavyi, V. G., and Mansurov, Y. N. (2016b). Analysis of the formation of multi-layer carbon nanotubes in the process of mechanical activation of the pyrolysis products of vegetable raw materials. *IOP Conf. Ser. Mat. Sci. Eng.* 127, 012008. doi:10.1088/1757-899X/127/1/012008

Sayed, E. T., Eisa, T., Mohamed, H. O., Abdelkareem, M. A., Allagui, A., Alawadhi, H., et al. (2019). Direct urea fuel cells: challenges and opportunities. *J. Power Sources* 417, 159–175. doi:10.1016/j.jpowsour.2018.12.024

Schneider, D., Escala, M., Supawittayayothin, K., and Tippayawong, N. J. I. (2011). Characterization of biochar from hydrothermal carbonization of bamboo. *Int. J. Energy Environ.* 2, 647–652.

Seh, Z. W., Kibsgaard, J., Dickens, C. F., Chorkendorff, I., Nørskov, J. K., and Jaramillo, T. F. (2017). Combining theory and experiment in electrocatalysis: insights into materials design. *Science* 355, eaad4998. doi:10.1126/science.aad4998

Shackley, S., Hammond, J., Gaunt, J., and Ibarrola, R. (2011). The feasibility and costs of biochar deployment in the UK. *Carbon Manag.* 2, 335–356. doi:10.4155/cmt.11.22

Shafizadeh, F. (1982). Introduction to pyrolysis of biomass. *J. Anal. Appl. Pyrolysis* 3, 283–305. doi:10.1016/0165-2370(82)80017-x

Shao, M., Chang, Q., Dodelet, J. P., and Chenitz, R. (2016). Recent advances in electrocatalysts for oxygen reduction reaction. *Chem. Rev.* 116, 3594–3657. doi:10.1021/acs.chemrev.5b00462

Sharifi, T., Hu, G., Jia, X., and Wågberg, T. (2012). Formation of active sites for oxygen reduction reactions by transformation of nitrogen functionalities in nitrogen-doped carbon nanotubes. *ACS Nano* 6, 8904–8912. doi:10.1021/nn302906r

Sharma, Y. C., Singh, B., and Korstad, J. (2011). A critical review on recent methods used for economically viable and eco-friendly development of microalgae as a potential feedstock for synthesis of biodiesel. *Green Chem.* 13, 2993–3006. doi:10.1039/c1gc15535k

Shen, D., Xiao, R., Gu, S., and Luo, K. (2011). The pyrolytic behavior of cellulose in lignocellulosic biomass: a review. *RSC Adv.* 1, 1641–1660. doi:10.1039/c1ra00534k

Shi, K., Yan, J., Lester, E., and Wu, T. (2014). Catalyst-free synthesis of multiwalled carbon nanotubes via microwave-induced processing of biomass. *Industrial Eng. Chem. Res.* 53, 15012–15019. doi:10.1021/ie503076n

Singh, S. K., Takeyasu, K., and Nakamura, J. (2019). Active sites and mechanism of oxygen reduction reaction electrocatalysis on nitrogen-doped carbon materials. *Adv. Mat.* 31, 1804297. doi:10.1002/adma.201804297

Su, X.-L., Cheng, M.-Y., Fu, L., Yang, J.-H., Zheng, X.-C., and Guan, X.-X. (2017). Superior supercapacitive performance of hollow activated carbon nanomesh with hierarchical structure derived from poplar catkins. *J. Power Sources* 362, 27–38. doi:10.1016/j.jpowsour.2017.07.021

Sun, L., Tian, C., Li, M., Meng, X., Wang, L., Wang, R., et al. (2013). From coconut shell to porous graphene-like nanosheets for high-power supercapacitors. *J. Mat. Chem. A* 1, 6462–6470. doi:10.1039/c3ta10897j

Sun, Z., Zheng, M., Hu, H., Dong, H., Liang, Y., Xiao, Y., et al. (2018). From biomass wastes to vertically aligned graphene nanosheet arrays: a catalyst-free synthetic strategy towards high-quality graphene for electrochemical energy storage. *Chem. Eng. J.* 336, 550–561. doi:10.1016/j.cej.2017.12.019

Suopajärvi, H., and Fabritius, T. (2013). Towards more sustainable ironmaking—an analysis of energy wood availability in Finland and the economics of charcoal production. *Sustainability* 5, 1188–1207. doi:10.3390/su5031188

Tang, C., Hu, Q., Li, F., He, C., Chai, X., Zhu, C., et al. (2018b). Coupled molybdenum carbide and nitride on carbon nanosheets: an efficient and durable hydrogen evolution electrocatalyst in both acid and alkaline media. *Electrochimica Acta* 280, 323–331. doi:10.1016/j.electacta.2018.05.129

Tang, C., and Qiao, S.-Z. (2019). 2D atomically thin electrocatalysts: from graphene to metallene. *Matter* 1, 1454–1455. doi:10.1016/j.matt.2019.10.023

Tang, C., Zhang, H., Xu, K., Hu, Q., Li, F., He, C., et al. (2018a). Scalable synthesis of heterostructure molybdenum and nickel sulfides nanosheets for efficient hydrogen generation in alkaline electrolyte, Catal. *Catal. Today* 316, 171–176. doi:10.1016/j.cattod.2018.03.010

Tang, C., Zhang, H., Xu, K., Zhang, Q., Liu, J., He, C., et al. (2019). Unconventional molybdenum carbide phases with high electrocatalytic activity for hydrogen evolution reaction. *J. Mat. Chem. A* 7, 18030–18038. doi:10.1039/c9ta04374h

Thompson, E., Danks, A. E., Bourgeois, L., and Schnepp, Z. (2015). Iron-catalyzed graphitization of biomass. *Green Chem.* 17, 551–556. doi:10.1039/c4gc01673d

Titirici, M.-M., White, R. J., Brun, N., Budarin, V. L., Su, D. S., del Monte, F., et al. (2015). Sustainable carbon materials. *Chem. Soc. Rev.* 44, 250–290. doi:10.1039/c4cs00232f

Uzun, B. B., Apaydın Varol, E., and Pütün, E. (2016). "Pyrolysis: sustain, way from biomass biofuels biochar," in *Biochar region. Suppl. Chain app*. Editors B. B. Uzun, E. Apaydın Varol, J. Liu, and V. J. Bruckman (Cambridge: Cambridge University Press), 239–265.

Vassilev, S. V., Baxter, D., Andersen, L. K., Vassileva, C. G., and Morgan, T. J. (2012). An overview of the organic and inorganic phase composition of biomass. *Fuel* 94, 1–33. doi:10.1016/j.fuel.2011.09.030

Vassilev, S. V., Baxter, D., Andersen, L. K., and Vassileva, C. G. (2010). An overview of the chemical composition of biomass. *Fuel* 89, 913–933. doi:10.1016/j.fuel.2009.10.022

Vassilev, S. V., Baxter, D., Andersen, L. K., and Vassileva, C. G. (2013). An overview of the composition and application of biomass ash. Part 1. Phase–mineral and chemical composition and classification. *Fuel* 105, 40–76. doi:10.1016/j.fuel.2012.09.041

Vassilev, S. V., Vassileva, C. G., and Baxter, D. (2014). Trace element concentrations and associations in some biomass ashes. *Fuel* 129, 292–313. doi:10.1016/j.fuel.2014.04.001

Vassilev, S. V., Vassileva, C. G., and Vassilev, V. S. (2015). Advantages and disadvantages of composition and properties of biomass in comparison with coal: an overview. *Fuel* 158, 330–350. doi:10.1016/j.fuel.2015.05.050

Vikkisk, M., Kruusenberg, I., Joost, U., Shulga, E., Kink, I., and Tammeveski, K. (2014). Electrocatalytic oxygen reduction on nitrogen-doped graphene in alkaline media. *Appl. Catal. B Environ.* 147, 369–376. doi:10.1016/j.apcatb.2013.09.011

Wang, B., Li, S., Wu, X., Liu, J., and Chen, J. (2016). Biomass chitin-derived honeycomb-like nitrogen-doped carbon/graphene nanosheet networks for applications in efficient oxygen reduction and robust lithium storage. *J. Mat. Chem. A* 4, 11789–11799. doi:10.1039/c6ta02858f

Wang, D.-W., Li, F., Yin, L.-C., Lu, X., Chen, Z.-G., Gentle, I. R., et al. (2012b). Nitrogen-doped carbon monolith for alkaline supercapacitors and understanding nitrogen-induced redox transitions. *Chem. Eur. J.* 18, 5345–5351. doi:10.1002/chem.201102806

Wang, J., Hao, J., Liu, D., Qin, S., Portehault, D., Li, Y., et al. (2017). Porous boron carbon nitride nanosheets as efficient metal-free catalysts for the oxygen reduction reaction in both alkaline and acidic solutions. *ACS Energy Lett.* 2, 306–312. doi:10.1021/acsenergylett.6b00602

Wang, J., Yue, X., Yang, Y., Sirisomboonchai, S., Wang, P., Ma, X., et al. (2020a). Earth-abundant transition-metal-based bifunctional catalysts for overall electrochemical water splitting: a review. *J. Alloys Compd.* 819, 153346. doi:10.1016/j.jallcom.2019.153346

Wang, K., Chen, H., Zhang, X., Tong, Y., Song, S., Tsiakaras, P., et al. (2020b). Iron oxide@graphitic carbon core-shell nanoparticles embedded in ordered mesoporous N-doped carbon matrix as an efficient cathode catalyst for PEMFC. *Appl. Catal. B Environ.* 264, 118468. doi:10.1016/j.apcatb.2019.118468

Wang, N., Tahmasebi, A., Yu, J., Xu, J., Huang, F., and Mamaeva, A. (2015). A Comparative study of microwave-induced pyrolysis of lignocellulosic and algal biomass. *Bioresour. Technol.* 190, 89–96. doi:10.1016/j.biortech.2015.04.038

Wang, S., Zhang, L., Xia, Z., Roy, A., Chang, D. W., Baek, J.-B., et al. (2012a). BCN graphene as efficient metal-free electrocatalyst for the oxygen reduction reaction. *Angew. Chem. Int. Ed.* 51, 4209–4212. doi:10.1002/anie.201109257

Wang, X., Wang, J., Wang, D., Dou, S., Ma, Z., Wu, J., et al. (2014b). One-pot synthesis of nitrogen and sulfur co-doped graphene as efficient metal-free electrocatalysts for the oxygen reduction reaction. *Chem. Commun.* 50, 4839–4842. doi:10.1039/c4cc00440j

Wang, Y., Duan, D., Ma, J., Gao, W., Peng, H., Huang, P., et al. (2019). Waste wine mash-derived doped carbon materials as an efficient electrocatalyst for oxygen reduction reaction. *Int. J. Hydrogen Energy* 44, 31949–31959. doi:10.1016/j.ijhydene.2019.10.100

Wang, Z., Li, P., Chen, Y., He, J., Zhang, W., Schmidt, O. G., et al. (2014a). Pure thiophene–sulfur doped reduced graphene oxide: synthesis, structure, and electrical properties. *Nanoscale* 6, 7281–7287. doi:10.1039/c3nr05061k

Wang, Z., Shen, D., Wu, C., and Gu, S. (2018). State-of-the-art on the production and application of carbon nanomaterials from biomass. *Green Chem.* 20, 5031–5057. doi:10.1039/c8gc01748d

Wu, J., Zheng, X., Jin, C., Tian, J., and Yang, R. (2015). Ternary doping of phosphorus, nitrogen, and sulfur into porous carbon for enhancing electrocatalytic oxygen reduction. *Carbon* 92, 327–338. doi:10.1016/j.carbon.2015.05.013

Wu, M., Wang, Y., Wei, Z., Wang, L., Zhuo, M., Zhang, J., et al. (2018a). Ternary doped porous carbon nanofibers with excellent ORR and OER performance for zinc–air batteries. *J. Mat. Chem. A* 6, 10918–10925. doi:10.1039/c8ta02416b

Wu, X., Li, S., Wang, B., Liu, J., and Yu, M. (2017). From biomass chitin to mesoporous nanosheets assembled loofa sponge-like N-doped carbon/g-C3N4 3D network architectures as ultralow-cost bifunctional oxygen catalysts. *Microporous Mesoporous Mater.* 240, 216–226. doi:10.1016/j.micromeso.2016.11.022

Wu, Z.-Y., Ji, W.-B., Hu, B.-C., Liang, H.-W., Xu, X.-X., Yu, Z.-L., et al. (2018b). Partially oxidized Ni nanoparticles supported on Ni-N co-doped carbon nanofibers as bifunctional electrocatalysts for overall water splitting. *Nano Energy* 51, 286–293. doi:10.1016/j.nanoen.2018.06.071

Xian, F., Gao, L., Zhang, Z., Zhang, H., Dong, S., and Cui, G. (2019). N, P dual-doped multi-wrinkled nanosheets prepared from the egg crude lecithin as the efficient metal-free electrocatalyst for oxygen reduction reaction. *Appl. Surf. Sci.* 476, 76–83. doi:10.1016/j.apsusc.2018.12.293

Xiao, F., Chen, Z., Wu, H., Wang, Y., Cao, E., Lu, X., et al. (2019). Phytic acid-guided ultra-thin N,P co-doped carbon coated carbon nanotubes for efficient all-pH electrocatalytic hydrogen evolution. *Nanoscale* 11, 23027–23034. doi:10.1039/c9nr07362k

Xiao, Z., Wang, Y., Huang, Y.-C., Wei, Z., Dong, C.-L., Ma, J., et al. (2017). Filling the oxygen vacancies in Co3O4 with phosphorus: an ultra-efficient electrocatalyst for overall water splitting. *Energy Environ. Sci.* 10, 2563–2569. doi:10.1039/c7ee01917c

Xiao, Z., Xie, C., Wang, Y., Chen, R., and Wang, S. (2021). Recent advances in defect electrocatalysts: preparation and characterization. *J. Energy Chem.* 53, 208–225. doi:10.1016/j.jechem.2020.04.063

Xing, T., Zheng, Y., Li, L. H., Cowie, B. C. C., Gunzelmann, D., Qiao, S. Z., et al. (2014). Observation of active sites for oxygen reduction reaction on nitrogen-doped multilayer graphene. *ACS Nano* 8, 6856–6862. doi:10.1021/nn501506p

Yaman, S. (2004). Pyrolysis of biomass to produce fuels and chemical feedstocks. *ChemInform* 35, 651–671. doi:10.1002/chin.200431298

Ye, D., Wang, L., Zhang, R., Liu, B., Wang, Y., and Kong, J. (2015). Facile preparation of N-doped mesocellular graphene foam from sludge flocs for highly efficient oxygen reduction reaction. *J. Mat. Chem. A* 3, 15171–15176. doi:10.1039/c5ta03060a

Yu, L., Huang, J., Li, Y., Jing, Y., Maliutina, K., Ma, R., et al. (2021). Electrochemical performance of low-temperature solid oxide fuel cells running on syngas from pyrolytic urban sludge. *Ceram. Int.* 47, 16956–16963. doi:10.1016/j.ceramint.2021.02.268

Zhang, B., Chen, R., Yang, Z., Chen, Y., Zhou, L., and Yuan, Y. (2019). Melamine-assisted synthesis of paper mill sludge-based carbon nanotube/nanoporous carbon nanocomposite for enhanced electrocatalytic oxygen reduction activity. *Int. J. Hydrogen Energy* 44, 31094–31103. doi:10.1016/j.ijhydene.2019.10.045

Zhang, H., Zhou, Z., Lei, Q., and Lo, T. W. B. (2023b). Recent advances in the operando structural and interface characterisation of electrocatalysts. *Curr. Opin. Electrochem.* 38, 101215. doi:10.1016/j.coelec.2023.101215

Zhang, J., He, J., Zheng, H., Li, R., and Gou, X. (2020a). N,S dual-doped carbon nanosheet networks with hierarchical porosity derived from biomass of Allium cepa as efficient catalysts for oxygen reduction and Zn–air batteries. *J. Mat. Sci.* 55, 7464–7476. doi:10.1007/s10853-020-04535-4

Zhang, J., Qu, L., Shi, G., Liu, J., Chen, J., and Dai, L. (2016c). N,P-Codoped carbon networks as efficient metal-free bifunctional catalysts for oxygen reduction and hydrogen evolution reactions. *Angew. Chem. Int. Ed.* 55, 2230–2234. doi:10.1002/anie.201510495

Zhang, J., Tahmasebi, A., Omoriyekomwan, J. E., and Yu, J. (2021). Microwave-assisted synthesis of biochar-carbon-nanotube-NiO composite as high-performance anode materials for lithium-ion batteries. *Fuel Process. Technol.* 213, 106714. doi:10.1016/j.fuproc.2020.106714

Zhang, J., Zhou, H., Liu, X., Zhang, J., Peng, T., Yang, J., et al. (2016b). Keratin-derived S/N co-doped graphene-like nanobubble and nanosheet hybrids for highly efficient oxygen reduction. *J. Mat. Chem. A* 4, 15870–15879. doi:10.1039/c6ta06212a

Zhang, L.-L., Tong, L., Ding, Y., Zhang, W., and Liang, H.-W. (2023a). Synthesis of hierarchically porous carbon materials by zinc salts-assisted carbonization of biomass and organic solid wastes. *Particuology* 84, 45–52. doi:10.1016/j.partic.2023.03.002

Zhang, L., and Xia, Z. (2011). Mechanisms of oxygen reduction reaction on nitrogen-doped graphene for fuel cells. *J. Phys. Chem. C* 115, 11170–11176. doi:10.1021/jp201991j

Zhang, M., Gao, B., Varnoosfaderani, S., Hebard, A., Yao, Y., and Inyang, M. (2013). Preparation and characterization of a novel magnetic biochar for arsenic removal. *Bioresour. Technol.* 130, 457–462. doi:10.1016/j.biortech.2012.11.132

Zhang, Q., Luo, F., Ling, Y., Xiao, S., Li, M., Qu, K., et al. (2020b). Identification of functionality of heteroatoms in boron, nitrogen and fluorine ternary-doped carbon as a robust electrocatalyst for nitrogen reduction reaction powered by rechargeable zinc–air batteries. *J. Mat. Chem. A* 8, 8430–8439. doi:10.1039/d0ta01572e

Zhang, Y., Lu, L., Zhang, S., Lv, Z., Yang, D., Liu, J., et al. (2018). Biomass chitosan derived cobalt/nitrogen doped carbon nanotubes for the electrocatalytic oxygen reduction reaction. *J. Mat. Chem. A* 6, 5740–5745. doi:10.1039/c7ta11258k

Zhang, Y., Zuo, L., Zhang, L., Huang, Y., Lu, H., Fan, W., et al. (2016a). Cotton wool derived carbon fiber aerogel supported few-layered MoSe2 nanosheets as efficient electrocatalysts for hydrogen evolution. *ACS Appl. Mat. Interfaces* 8, 7077–7085. doi:10.1021/acsami.5b12772

Zhao, B., Wang, X., and Yang, X. (2015). Co-Pyrolysis characteristics of microalgae isochrysis and chlorella: kinetics, biocrude yield and interaction. *Bioresour. Technol.* 198, 332–339. doi:10.1016/j.biortech.2015.09.021

Zhao, N. Q., He, C. N., Du, X.-W., Shi, C., Li, J. J., and Cui, L. (2006). Amorphous carbon nanotubes fabricated by low-temperature chemical vapor deposition. *Carbon* 44, 1859–1862. doi:10.1016/j.carbon.2006.03.010

Zhao, X., Zhang, Q., Chen, C.-M., Zhang, B., Reiche, S., Wang, A., et al. (2012). Aromatic sulfide, sulfoxide, and sulfone mediated mesoporous carbon monolith for use in supercapacitor. *Nano Energy* 1, 624–630. doi:10.1016/j.nanoen.2012.04.003

Zhao, Y., Wan, J., Yao, H., Zhang, L., Lin, K., Wang, L., et al. (2018). Few-layer graphdiyne doped with sp-hybridized nitrogen atoms at acetylenic sites for oxygen reduction electrocatalysis. *Nat. Chem.* 10, 924–931. doi:10.1038/s41557-018-0100-1

Zheng, X., Cao, X., Li, X., Tian, J., Jin, C., and Yang, R. (2017). Biomass lysine-derived nitrogen-doped carbon hollow cubes via a NaCl crystal template: an efficient bifunctional electrocatalyst for oxygen reduction and evolution reactions. *Nanoscale* 9, 1059–1067. doi:10.1039/c6nr07380h

Zheng, X., Cao, X., Wu, J., Tian, J., Jin, C., and Yang, R. (2016). Yolk-shell N/P/B ternary-doped biocarbon derived from yeast cells for enhanced oxygen reduction reaction. *Carbon* 107, 907–916. doi:10.1016/j.carbon.2016.06.102

Zheng, Y., Jiao, Y., Zhu, Y., Li, L. H., Han, Y., Chen, Y., et al. (2014). Hydrogen evolution by a metal-free electrocatalyst. *Nat. Commun.* 5, 3783. doi:10.1038/ncomms4783

Zhou, Q., Ju, W., Yong, Y., Zhang, Q., Liu, Y., and Li, J. (2020). Effect of the N/P/S and transition-metal co-doping on the quantum capacitance of supercapacitor electrodes based on mono- and multilayer graphene. *Carbon* 170, 368–379. doi:10.1016/j.carbon.2020.08.045

Glossary

AFM	Atomic force microscopy
AI	Artificial intelligence
CNs	Carbon nanomaterials
CNTs	Carbon nanotubes
CNFs	Carbon nanofibres
CO2RR	Carbon dioxide reduction reaction
CV	Cyclic voltammetry
CVD	Chemichal vapour deposition
DFT	Density functional theory
EDS	Energy-dispersive X-ray spectroscopy
EIS	Electrochemical impedance spectroscopy
ENPs	Engineered nanoparticles
EPR	Electron paramagnetic resonance
FC	Fuel cell
HER	Hydrogen evolution reaction
HOR	Hydrogen oxidation reaction
HPCs	Hierarchically porous carbons
HTC	Hydrothermal carbonization
IR/FT-IR	Infrared/Fourier-transform infrared spectroscopy
LCA	Life-cycle assessment
LSV	Linear sweep voltammetry
MOF	Metal organic framework
NPs	Nanoparticles
SSA	Specific surface area
TMs	Transition metals
QD	Quantum dot
OER	Oxygen evolution reaction
ORR	Oxygen reduction reaction
SEM/ FE-SEM	Scanning electron microscopy/field-emission scanning electron microscopy
TEM/ HR-TEM	Transmission electron microscopy/high-resolution transmission electron microscopy
XAFS	X-ray absorption fine structure
XPS	X-ray photoelectron spectroscopy
XRD	X-ray power diffraction
UV-vis	Ultraviolet–visible spectroscopy